Department of Physics and Astronomy

University of Heidelberg

Master thesis

in Physics

submitted by

Anja Butter

born in Mayen

2014

Constraining the NMSSM with LHC and Planck

This Master thesis has been carried out by Anja Butter

at the

Institute for Theoretical Physics

under the supervision of

Herrn Prof. Dr. Tilman Plehn

and

Herrn Dr. Dirk Zerwas

Laboratoire de l'Accélérateur Linéaire, Université Paris-Sud, Orsay

Einschränkung des NMSSM mit LHC und Planck

Die Beobachtung von Physik jenseits des Standard Models wie dunkler Materie führten zur Entwicklung neuer Theorien wie Supersymmetrie. Die vorliegende Arbeit untersucht die Möglichkeit das NMSSM, ein supersymmetrisches Model, anhand der Ergebnisse von Experimenten in den Bereichen dunkle Materie, am LHC sowie zum anomalen magnetischen Moment des Muons einzuschränken. Dazu wurde NMSSMTools, ein Program zur Berechnung des Massenspektrum sowie weiterer Observablen im NMSSM, in SFitter eingebunden. In einer Studie des NMSSM im Grenzfall des MSSM können wir mSUGRA in den h und A-funnel Regionen innerhalb von 10% Abweichung in das CNMSSN einbetten. Ausgehend von diesen Punkten untersuchen wir den Einfluss der zusätzlichen NMSSM Parameter, die den Parameterraum im Vergleich zum MSSM erweitern, in Likelikood Fits unter Nutzung der Frequentist Methode.
In der h-funnnel Region finden wir zwei Regionen, die mit den Messungen zu dunkler Materie und der Higgs Masse übereinstimmen. In einer Region ist das Singlet entkoppelt und in der anderen besteht das zweit schwerste Higgs im wesentlichen aus dem Singletanteil. Der best-fit Punkt der A-funnel Region vergrößert sich zu einem Bereich in der λ-κ-Ebene, mit einem konstanten Verhältnis von λ zu κ.

Constraining the NMSSM with LHC and Planck

The observation of physics beyond the Standard Model like dark matter lead to the development of new theories like supersymmetry. The present thesis studies the possibility to constrain the NMSSM, a supersymmetric model, using experimental measurements obtained from dark matter searches, the LHC and studies of the anomalous magnetic moment. NMSSMTools, a program to calculate the mass spectrum and additional observables for the NMSSM, is implemented in SFitter. Studying the NMSSM in the limit of the MSSM, we are able to embed mSUGRA in the CNMSSM in the h and A-funnel region within 10 % error. Using the reproduced results as start points we investigate the impact of the additional NMSSM variables, that extend the parameter space with respect to the MSSM, in likelihood fits using the frequentist method.
For the h-funnel region we find two regions consistent with the dark matter and Higgs mass measurements, one with a decoupled singlet and one where the second heaviest Higgs is singlet like. For the A-funnel region the best fitting point enlarges into a region in λ-κ -plane that corresponds to a constant ratio of λ/κ.

Contents

1 Introduction

The Standard Model of Particle Physics (SM) [1] is one of the most successful theories ever developed to describe nature. It describes the universe at its innermost principles by postulating its elementary particles and the mechanisms by which they interact with each other. Predicting the outcome of a huge variety of experiments with results varying over many orders of magnitude, it is the most precisely measured theory that exists.

On the other hand we encounter deviations of experimental results from theoretical predictions and further unsolved problems. One of the best known examples is the existence of dark matter that can only be measured due to its gravitational impact but represents 26.8% [2] of the mass-energy of the universe. As it remains invisible for optical research methods, its electromagnetic interaction must be very weak. Adhering to a description with elementary particles, its massive constituents can not be provided by the SM.

The intriguing difference of 3.6 σ between the theoretical prediction of the anomalous magnetic moment of the muon and its measurement [3] provokes as well speculations about physics beyond the SM.

One last example is the ATLAS/CMS [4] discovery of a new particle, in agreement with the SM expectation of a Higgs particle, that gives rise to unanswered questions. In fact the Higgs mass can not be deduced from first principles in the SM and it is by no means clear why the mass is so small compared to the grand unification (GUT) scale.

The mentioned problems make it necessary to develop new theories. To be successful, a new theory has to describe the so far unsolved problems in addition to the data that are already well described by the SM. Therefore it suggests itself to just extend the SM, which is where supersymmetry [5] comes into play. It embeds the SM into a model where every SM particle has a supersymmetric partner [6]. Supersymmetry has become one of the most popular theories to solve the discrepancies because of its capability to unify the couplings of the three interactions and the fact that the lightest supersymmetric particle (LSP) provides a good dark matter candidate. The simplest supersymmetric model in the sense of particle multiplicity is the minimal supersymmetric extension of the SM (MSSM) [7] as it is built with the minimal amount of additional particles that are necessary to form a supersymmetric theory. The MSSM has been studied in detail by many scientists with promising results. But as no supersymmetric partner has been found this leaves open space for more complex models like the NMSSM[8].

By adding one additional singlet to the MSSM, the NMSSM, the next to minimal supersymmetric extension of the Standard Model, benefits from a richer phenomenology in the especially interesting Higgs sector.

The purpose of this thesis is to study the phenomenology of the NMSSM in the limit of a semi constrained model. We focus on the h-funnel and A-funnel regions that can provide the correct relic density. Both regions have been the objectiv of MSSM studies. First we consider the NMSSM in the MSSM limit by decoupling the introduced singlet for the two regions.

Starting from mSUGRA best-fit points we explore the phenomenology of the NMSSM under consideration of the above mentioned measurements. We use SFitter [9] to fit the semi constrained NMSSM to the data for a given parameter space by maximizing the corresponding log-likelihood.

2 Beyond the Standard Model

2.1 Why Supersymmetry? A Short Motivation

The Standard Model of particle physics (SM) [1] has been developed during the last century and describes all known matter particles and their interactions on the quantum level. Although most of its predictions can be verified today with an unprecedented accuracy, some discrepancies as well as unsolved problems remain experiment-wise as well as theory-wise. The most famous ones arise from astronomical observations and concern the existence of dark matter and dark energy that can not be explained with the SM. Others, like the fact that general relativity is not included in the SM or the tension between the predicted value of the anomalous magnetic moment and its measurement [3] give further evidence that the SM is not the final solution.

The problem at which we will take a close look is the so called Hierarchy Problem. For its description and the introduction to the MSSM I will follow the conventions and methods of S.P. Martin's Supersymmetry Primer [5]. When we compute the loop corrections to the propagator of the Higgs Boson in the Standard Model we basically encounter three contributions: those of the fermions like the top quark (Fig. 2.1a), those of the Higgs itself (Fig. 2.1b) and those of the W/Z Boson. These result in quadratically divergent contributions on the cutoff scale Λ to the bare Higgs mass:

$$m_H^2 = m_{H,0}^2 + \frac{3g^2}{32\pi^2}\frac{\Lambda^2}{m_W^2}\left(m_H^2 + 2m_W^2 + m_Z^2 - \frac{4}{3}m_t^2\right) \text{[10]} \tag{2.1}$$

If we want to compensate for these contributions by introducing a counterterm we have to face two problems. On the one hand the counterterm would strongly

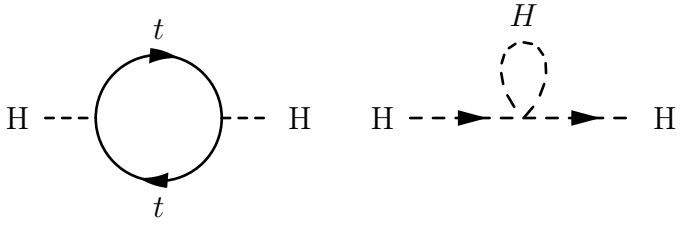

(a) (b)

Figure 2.1: Corrections to the Higgs propagator coming from the top quark (a) and the Higgs boson (b).

depend on the exact value of the cutoff scale, as it does not enter logarithmically. On the other hand the cancellation has to be very precise, e.g. when we assume $\Lambda = Q_{Planck}$, the counterterm has to be of the order of $10^{2\times 19}\,\mathrm{GeV}^2$ and cancel with the loop corrections to generate a term of the order of $10^4\,\mathrm{GeV}^2$. This requires an extreme fine tuning.

In order to avoid this fine tuning, supersymmetry [6] makes use of the different signs that we observe in equation 2.1. While the bosons enter with a positive sign the top quark as every other fermion gives a negative contribution. This means we can avoid the finetuning by introducing a systematic cancellation of the bosonic and fermionic terms that diverge with Λ^2.

Therefore we have to assign a bosonic partner to each SM fermion and a fermionic partner to each boson. In other words, one introduces a transformation that turns a bosonic state into a fermionic one and vice versa while keeping the gauge charges identical. The corresponding symmetry is called supersymmetry.

To account for the SUSY transformation it turns out to be convenient to combine SM particles and their supersymmetric partners in a common structure, a supermultiplet. A chiral supermultiplet combines a complex scalar field and a Weyl fermion and is therefore used for the SM quarks and leptons and the Higgs particles. The gauge bosons and their partners are represented by gauge supermultiplets that contain a spin 1 vector boson and again a spin 1/2 Weyl fermion.

The starting point for every model is the superpotential that is written in terms of these supermultiplets. A theory containing all SM particles can be derived from

$$W_{MSSM} = \mathbf{h_u}\hat{H}_u\hat{Q}\hat{U}_R^C - \mathbf{h_d}\hat{H}_d\hat{Q}\hat{D}_R^C - \mathbf{h_e}\hat{H}_d\hat{L}\hat{E}_R^C + \mu\hat{H}_u\hat{H}_d. \tag{2.2}$$

We can identify the chiral supermultiplets for the left handed and right handed quarks $(\hat{Q}, \hat{U}_R^C, \hat{D}_R^C)$, two for the Higgs $(\hat{H}_u, \hat{H}_d)$, the Yukawa coupling $(\mathbf{h_i})$ and a dimensionfull parameter (μ). The two different doublet chiral supermultiplets for the Higgs are necessary as the charges of the fields have to add up to zero for up as well as down-type quarks. Otherwise the terms would not be gauge invariant under the electromagnetic transformation. The gauge multiplets enter into the Lagrangian through the usual covariant derivatives when we make our Lagrangian gauge invariant under U(1), SU(2) and SU(3).

Starting from the superpotential one obtains the scalar potential of the theory by adding the derivatives of the superpotential with respect to all scalar fields (ϕ_i) :

$$V(\phi, \phi^*) = W^i W_i^* \left(+\frac{1}{2}\sum_a g_a^2(\phi^* T^a \phi)^2 \right) \qquad \text{with} \quad W^i = \frac{\delta W}{\delta \phi_i} \tag{2.3}$$

The second term arises from gauge interaction. g_a is the gauge coupling and T^a are the hermitian matrices that represent the gauge groups.

A full description of how to derive the complete Lagrangian from the superpotential can be found under [5].

If we want to adopt supersymmetry we encounter a major problem. If supersymmetry was implemented in the described way, each supersymmetric partner of a SM particle would have the same mass as the SM particle and would have been discovered long time ago. Supersymmetry thus has to be broken. In order to continue to provide a solution for the hierarchy problem, the SUSY breaking terms that we insert into the Lagrangian must not affect the coupling of SUSY particles, as the contributions to the Higgs mass in eq.2.1 - although written in terms of the masses - are determined by the coupling. Nevertheless we can introduce soft SUSY breaking mass terms that leave the coupling unchanged but can push the masses to higher values and finally out of the so far detectable mass range.

In the next section we will take a look at an actual implementation of supersymmetry and its phenomenology.

2.2 The MSSM

2.2.1 The Particle Content

The Minimal Supersymmetric Standard Model contains the minimal number of particles that is necessary to construct a supersymmetric version of the SM. According to section 2.1 we introduce spin-0 sleptons and squarks as supersymmetric partners of the SM fermions and spin-1/2 gauginos as partners of the spin-1 gauge bosons. For the Higgs sector we have to introduce two $SU(2)_L$ doublet chiral supermultiplets, one for the up-type quarks and one for down-type quarks and leptons. One doublet consist (e.g. H_u) hence of two complex or four real scalar fields (H_u^+, H_u^0) and two Weyl fermions $(\tilde{H}_u^+, \tilde{H}_u^0)$

Why two Higgs doublets?

$$\left[\begin{pmatrix} H_u^+ \\ \tilde{H}_u^+ \end{pmatrix} \begin{pmatrix} H_u^0 \\ \tilde{H}_u^0 \end{pmatrix}\right], \quad \left[\begin{pmatrix} H_d^0 \\ \tilde{H}_d^0 \end{pmatrix} \begin{pmatrix} H_d^- \\ \tilde{H}_d^- \end{pmatrix}\right] \tag{2.4}$$

These fields mix into mass eigenstates. On the bosonic side we start with 8 real scalar fields. Three of them have to be Goldstone bosons that become the longitudinal degrees of freedom of the $W^\pm$ and Z^0 bosons. The two remaining charged fields combine to form a charged Higgs boson $H^\pm$. So we are left with three neutral scalar fields. Two of them are CP-even bosons h_1^0 and h_2^0, one of them being usually SM like, and the last one is a CP-odd scalar field A_1^0.

Combining up and down-type Higgsinos we find two neutral fermions, that mix with the two neutral gauginos $\tilde{W}^0$ (wino) and $\tilde{B}^0$ (bino) into four mass eigenstates, so called neutralinos. Additionally we find two charged fermions $\tilde{H}_u^+$ and $\tilde{H}_d^-$. They mix with the $\tilde{W}^\pm$ into two charginos, charged mass eigenstates.

An overview can be found under neutralinos and charginos in Table 2.1.

For the left and right handed component of every quark we introduce separate partners. These mix into non degenerate mass eigenstates. This leaves us with two scalar squarks for each quark. The same is true for the electron, muon and tau.

	SM Particle (R=+1)			SUSY Partner(R=-1)		
Names	Gauge ES	Mass ES	Spin	Gauge ES	Mass ES	Spin
quarks / squarks	$u_{L/R}, c_{L/R}, t_{L/R}$	u, c, t	1/2	$\tilde{u}_{L/R}, \tilde{c}_{L/R}, \tilde{t}_{L/R}$	$\tilde{u}_{1/2}, \tilde{c}_{1/2}, \tilde{t}_{1/2}$	0
	$d_{L/R}, s_{L/R}, b_{L/R}$	d, s, b	1/2	$\tilde{d}_{L/R}, \tilde{s}_{L/R}, \tilde{b}_{L/R}$	$\tilde{d}_{1/2}, \tilde{s}_{1/2}, \tilde{b}_{1/2}$	0
lepton / sleptons	$e_{L/R}, \mu_{L/R}, \tau_{L/R}$	e, μ, τ	1/2	$\tilde{e}_{L/R}, \tilde{\mu}_{L/R}, \tilde{\tau}_{L/R}$	$\tilde{e}_{1/2}, \tilde{\mu}_{1/2}, \tilde{\tau}_{1/2}$	0
	ν_e, ν_μ, ν_τ	ν_e, ν_μ, ν_τ	1/2	$\tilde{\nu}_e, \tilde{\nu}_\mu, \tilde{\nu}_\tau$	$\tilde{\nu}_e, \tilde{\nu}_\mu, \tilde{\nu}_\tau$	0
neutralinos	W^0, B^0	Z^0, γ	1	$\tilde{W}^0, \tilde{B}^0$	$\tilde{\chi}^0_1, \tilde{\chi}^0_2, \tilde{\chi}^0_3, \tilde{\chi}^0_4$	1/2
	H^0_u, H^0_d	h^0_1, h^0_2, A^0_1	0	$\tilde{H}^0_u, \tilde{H}^0_d$		
charginos	$W^\pm$	$W^\pm$	1	$\tilde{W}^\pm$	$\tilde{\chi}^\pm_1, \tilde{\chi}^\pm_2$	1/2
	H^+_u, H^-_d	$H^\pm$	0	$\tilde{H}^+_u, \tilde{H}^-_d$		
gluon / gluino	g	g	1	$\tilde{g}$	$\tilde{g}$	1/2

Table 2.1: Overview of SM particles and their supersymmetric partners in the MSSM

The influence of the neutrino sector on SUSY observables like the LSP or the Higgs masses is negligible. For practical purpose we only assume three sneutrinos (partners of the left handed neutrinos) for which the mass eigenstate coincides with their gauge eigenstate, neglecting the possibility of right handed neutrinos [11].

Finally there are eight massless gluons and their mass degenerate superpartners that are called gluinos. Summing up we are left with 31 undetected massive particles.

2.2.2 The Mass Spectrum of the MSSM

In the last section we have identified the particles that arise for the minimal supersymmetric extension of the SM. Now we will see how their masses depend on the SUSY breaking parameters.

We start by writing down the most general expression for SUSY breaking terms in the MSSM. Therefore one has to consider three classes of soft-breaking terms:

1. Scalar mass terms
2. Trilinear scalar interactions
3. Gaugino mass terms

Hence the Lagrangian contains additional mass terms for gauginos, squarks, sleptons and the Higgs bosons and a mixing term that relates H_u and H_d. The second class introduces trilinear scalar interactions between the Higgs and the squarks and slepton. The SUSY breaking mass terms and the trilinear SUSY breaking couplings are 3×3 matrices in family space like the Yukawa couplings in the superpotential. Finally the gaugino mass terms contain the SUSY breaking masses for gluinos, winos and binos.

Summing up all terms we find:

$$\begin{aligned} L_{soft}^{MSSM} = & - \tilde{Q}^{\dagger}\mathbf{m_Q^2}\tilde{Q} - \tilde{L}^{\dagger}\mathbf{m_L^2}\tilde{L} - \tilde{\bar{u}}^{\dagger}\mathbf{m_{\bar{u}}^2}\tilde{\bar{u}}^{\dagger} - \tilde{\bar{d}}^{\dagger}\mathbf{m_{\bar{d}}^2}\tilde{\bar{d}}^{\dagger} - \tilde{\bar{e}}^{\dagger}\mathbf{m_{\bar{e}}^2}\tilde{\bar{e}}^{\dagger} \\ & - m_{H_u}^2 H_u^* H_u - m_{H_d}^2 H_d^* H_d - (m_3^2 H_u H_d + c.c.) \\ & - (\tilde{\bar{u}}\mathbf{h_u}\mathbf{A_u}\tilde{Q}H_u + \tilde{\bar{d}}\mathbf{h_d}\mathbf{A_d}\tilde{Q}H_d + \tilde{\bar{e}}\mathbf{h_e}\mathbf{A_e}\tilde{L}H_d + c.c.) \\ & - \frac{1}{2}(M_3\tilde{g}\tilde{g} + M_2\tilde{W}\tilde{W} + M_1\tilde{B}\tilde{B} + c.c.) \end{aligned} \tag{2.5}$$

So far we made no assumption about the origin of these terms. Instead we only state that there is a hidden sector which causes SUSY breaking and which interacts with the MSSM in such a way that the SUSY breaking can be transferred from the hidden sector to the MSSM. One of the most investigated models is mSUGRA [12] where the breaking occurs due to a flavour blind and purely gravitational interaction between the hidden sector and the MSSM. This model has the advantage of only 5 input parameters: $m_0, m_{1/2}, A_0, tan\beta$ and the sign of μ. m_0 and $m_{1/2}$ are the unified masses of the scalars and gauginos at the GUT scale. A_0 is the unifies the trilinear couplings at the GUT scale and $\tan\beta$ is the ratio of the two vacuum expectation values, the only parameter given at the electroweak scale. All unification parameters set the values of the masses and couplings at the GUT scale. To evaluate the mass spectrum at the electroweak scale we have to run the unified couplings and susy breaking masses separately to the electroweak scale where the parameters are no longer unified due to their RGEs that differ depending on the considered parameter. As we will later analyse a similar model for the more complex NMSSM case, it is instructive to see how the masses of the SUSY particles depend on the input parameters for the mSUGRA case.

Higgs

The Higgs boson has a special position in the Standard Model. Due to electroweak symmetry breaking the Higgs acquires a non vanishing vacuum expectation value (vev). Therefore it gives mass to the Z and W boson and the quarks and leptons proportional to their Yukawa coupling to the Higgs. The mass of Higgs itself is determined by its vev and the Higgs self-coupling. In the MSSM we have two CP even, one CP odd and one charged Higgs. Their tree level Higgs masses can be calculated using the soft SUSY breaking parameters m_{H_u}, m_{H_d} and μ. m_{H_u} and m_{H_d} in turn are unified to m_0 at the GUT scale and we have to run them with the renormalization group equations to obtain their value at the electroweak scale. Using the soft input parameters the tree level masses are

$$m_{A_1}^2 = 2\left|\mu\right|^2 + m_{H_u}^2 + m_{H_d}^2 \tag{2.6}$$

$$m_{h_1,h_2}^2 = \frac{1}{2}\left(m_{A_1}^2 + m_Z^2 \mp \sqrt{(m_{A_1}^2 - m_Z^2)^2 + 4m_{A_1}^2 m_Z^2 \sin^2 2\beta}\right) \tag{2.7}$$

$$m_{H^{\pm}}^2 = m_{A_1}^2 + m_W^2. \tag{2.8}$$

While m_{A_1}, m_{h_2} and $m_{H^\pm}$ can in principle become arbitrarily large - apart from the fact that the SUSY breaking terms will no longer be soft at some point - the mass of the lightest Higgs is limited by $m_{h_1} < m_Z \left|\cos 2\beta\right|$. Loop contributions from the stop squarks are in principle able to increase this value at one loop level if the stop squarks are sufficiently heavy [13].

Squarks and Sleptons

The masses of the squarks and sleptons are determined as eigenvalues of mass matrices that in principle allow for mixinq of all scalars with the same quantum numbers. Due to experimental evidence as the branching ratio $\mu \to e\gamma$ [14] we know that most of the mixing angles have to be very small so that we can assume the mixing matrices to be diagonal for the first and second generation.

mSUGRA assumes the unification of the squark and slepton masses at the GUT scale. This means that the mass at the other scales can be parametrized by the distance from the GUT scale.
In the case of the right handed up-type squark this results in

$$m^2_{\tilde{u}_{1,2}} = m_0^2 + K_3 + \frac{4}{9}K_1 \quad \text{with} \quad K_a(Q) = \begin{pmatrix} 3/5 \\ 3/4 \\ 4/3 \end{pmatrix} \frac{1}{2\pi^2} \int_{\ln Q}^{\ln Q_0} g_a^2(t) \left|M_a(t)\right|^2 \mathrm{d}t. \tag{2.9}$$

$g_a^2(t)$ are the couplings of the three different forces and $|M_a(t)|^2$ the SUSY breaking masses of the corresponding sfermions evaluated at the scale t. The prefactor $\frac{4}{9}$ corresponds to the squared electromagnetic charge of an up-type quark. The factors K_a are the same for all squarks and sleptons and only the prefactors change depending on the charges of the sparticles under the gauge group.

The stronger Yukawa coupling of the third generation and the soft scalar coupling cause a non negligible mixing for the third generation, as one can see in the off diagonal terms of its mixing matrix.

why are the off-diagonal terms porportional to the vev?

$$\mathbf{m^2_{\tilde{t}}} = \begin{pmatrix} m^2_{Q_3} + m_t^2 + (\frac{1}{2} - \frac{2}{3}\sin^2\theta_W)\cos(2\beta)m_Z^2 & v(a_t^* \sin\beta - \mu y_t \cos\beta) \\ v(a_t \sin\beta - \mu^* y_t \cos\beta) & m^2_{\tilde{u}_3} + m_t^2 + (\frac{2}{3}\sin^2\theta_W)\cos(2\beta)m_Z^2 \end{pmatrix} \tag{2.10}$$

The off diagonal terms depend on the mass of the top quark $m_t = y_t v$ and can be hence of the same order of magnitude as the diagonal terms. Hence the masses of the stops have to be determined in an additional step as Eigenvalues of their mixing matrix.

Neutralinos and Charginos

The tree level contributions to the neutralino and chargino masses consist of the soft breaking terms proportional to M_1, M_2 and μ and the coupling between Higgs

bosons and gauginos evaluated around the vev. A first approximation evaluating the Eigenvalues of the tree level mass matrices identifies one neutralino mass of the order of M_1, a neutralino and a chargino with masses of about M_2 and the masses of two neutralinos and one chargino whose absolute values are roughly M_3.

Especially the mass of the lightest neutralino is very important for further studies, as it is the most likely candidate for dark matter in supersymmetric models [15].

The beta functions of the running masses $M_i (i = 1, 2, 3)$ reveal that M_i/g_i^2 remains scale independent for one loop corrections. Moreover the running coupling constants g_i tend to cross each other [16] roughly at the same scale around $2 \times 10^{16}\,\mathrm{GeV}$ so that we can impose unification at the GUT scale to g_U. Adding the mSUGRA assumption, that the M_i unify at the GUT scale to $m_{1/2}$ leads to the correlation

$$\frac{M_1}{g_1^2} = \frac{M_2}{g_2^2} = \frac{M_3}{g_3^2} = \frac{m_{1/2}}{g_U^2} \tag{2.11}$$

that is now valid for all scales.

Using the known ratios of the coupling constants at the SUSY scale, the mass parameters are related by

$$M_1 : M_2 : M_3 = 1 : \frac{3}{5}\tan^{-2}\theta_W : \frac{3}{5}\frac{\alpha_s}{\alpha}\cos^2\theta_W = 1 : 2 : 6. \tag{2.12}$$

This implies a mass hierarchy that allows us to identify the masses of the neutralinos and charginos as $m_{\chi_1^0} \approx M_1$, $m_{\chi_2^0} \approx m_{\chi_1^\pm} \approx M_2$ and $\left|m_{\chi_3^0}\right| \approx \left|m_{\chi_4^0}\right| \approx \left|m_{\chi_2^\pm}\right| \approx |\mu|$.

Now we can use the leading order RGE of M_2 to give a very rough estimation of the mass of the LSP in terms of the input parameter $m_{1/2}$. The leading order of the RGE is

$$16\pi^2 \frac{dM_2}{d\ln Q^2} = g_2^2 M_2. \tag{2.13}$$

Using $M_2(Q_{GUT}) = m_{1/2}$ we find

$$\frac{m_{1/2}}{M_2(Q)} = \left(\frac{Q_{GUT}}{Q}\right)^{\frac{2g_2^2}{16\pi^2}}. \tag{2.14}$$

under the assumption of a scale independent coupling g_2. Evaluating this expression around the SUSY scale we can estimate a typical ratio for $m_{1/2}(Q_{GUT})/M_2(Q_{SUSY})$ of about 1.2. This allows us finally to express the LSP mass directly in terms of $m_{1/2}$.

$$m_{\chi_1^0} \approx M_1(Q_{SUSY}) = \frac{M_2(Q_{SUSY})}{2} = \frac{m_{1/2}}{2 \times 1.2} = \frac{m_{1/2}}{2.4} \tag{2.15}$$

Gluino

In the same way we can do a first order approximation for the gluino [17] mass

$$m_{\tilde{g}} = M_3 = \frac{m_{1/2} \times 3}{1.2} \tag{2.16}$$

that is considerably heavier than the neutralino and chargino masses. However there are additional contributions that cause sizeable deviations from this value due to the strong coupling at one loop level.

2.2.3 The μ Problem

A rather intriguing parameter that appeared during the discussion of the MSSM is the μ parameter. It appears the first time in the superpotential in eq. 2.2 as a dimensionfull parameter in the Higgs mass term. It is in that sense special, that it is the only dimensionfull parameter that does not break supersymmetry. As it does not arise from SUSY breaking, this parameter is not connected to the SUSY breaking scale. Therefore a natural choice would be a value around the GUT scale, that is the only other scale that we have.

Yet it turns out, that we can find an expression for μ when we minimize the Higgs potential of the MSSM. Collecting only those terms that are quadratic in the neutral Higgs fields and contain no other field - otherwise the term vanishes in the minimum - we find an expression for the potential in the minimum:

$$V = \left(|\mu|^2 + m_{H_u}^2\right)\left|H_u^0\right|^2 + \left(|\mu|^2 + m_{H_d}^2\right)\left|H_d^0\right|^2 \tag{2.17}$$

$$- \left(m_3^2 H_u^0 H_d^0 + c.c.\right) + \frac{1}{8}(g^2 + g'^2)\left(\left|H_u^0\right|^2 - \left|H_d^0\right|^2\right)^2 \tag{2.18}$$

Using the minimization conditions $\partial V/\partial H_u^0 = 0$ and $\partial V/\partial H_d^0 = 0$ one finds two equations:

$$\sin(2\beta) = \frac{2m_3^2}{m_{H_u}^2 + m_{H_d}^2 + 2\left|\mu\right|^2} \tag{2.19}$$

$$m_Z^2 = m_{H_u}^2\left(\frac{1}{\cos(2\beta)} - 1\right) - m_{H_d}^2\left(\frac{1}{\cos(2\beta)} + 1\right) - 2\left|\mu\right|^2 \tag{2.20}$$

The squared Z mass is approximately $8300\,\mathrm{GeV}^2$. At the same time $m_{H_u}^2$ and $m_{H_d}^2$ are SUSY breaking parameters. In mSUGRA they are unified at the GUT scale. With the renormalization group equations one evolves their values to the SUSY breaking scale where one typically finds values of about $10^6\,\mathrm{GeV}^2$. These high values are mainly driven by the high stop masses. They now have to cancel with the SUSY respecting parameter μ that has no reason to be around the SUSY breaking scale. Moreover it is necessary that this cancellation happens at least at percent

	MSSM	mSUGRA
Yukawa couplings	$\mathbf{h_u}, \mathbf{h_d}, \mathbf{h_e}$	
Dimensionfull SUSY parameter	μ	$sgn(\mu)$
Corresponding s.br. parameter	$m_3^2 (\equiv B\mu)$	
Ratio of vevs	$\tan\beta$	$\tan\beta$
Higgs masses (s.br.)	$m_{H_u}^2, m_{H_d}^2$	m_0
Squark and slepton masses (s.br.)	$\mathbf{m_Q^2}, \mathbf{m_U^2}, \mathbf{m_D^2}, \mathbf{m_L^2}, \mathbf{m_E^2}$	m_0
Trilinear couplings (s.br.)	$\mathbf{A_u}, \mathbf{A_d}, \mathbf{A_e}$	A_0
Gaugino masses (s.br.)	M_1, M_2, M_3	$m_{1/2}$

Table 2.2: Supersymmetric parameters for the MSSM and their unified parameters in mSUGRA. SUSY breaking parameters are labelled s.br.

level to generate the Z mass term. We call this fine tuning problem the μ-problem.

In the context of gravity mediated supersymmetry breaking the Giudice-Masiero mechanism [18] can provide a solution to the μ-problem. It introduces an additional operator in the Kähler potential.

That is really too short to make a lot of sense…

$$K \supset \frac{\lambda_\mu}{M_P} H_u H_d X^* + c.c. \tag{2.21}$$

λ_μ is a dimensionless coupling and X is a chiral field. It is the messenger whose auxiliary field F is responsible for SUSY breaking. If F acquires a vev we can reproduce the μ-term with $\mu = \frac{\lambda_\mu}{M_P} < F_X^* >$. As a typical value of the vev in the low energy limit is $< F_X^* > \approx m_{soft} M_P$, we end up with a μ value at the order of the desired soft SUSY breaking scale.

2.2.4 Summary

In this section we have introduced supersymmetry on the basis of the MSSM. We found that the extension to supersymmetry is highly predictive, as all couplings are already determined by the SM. It is only after the introduction of SUSY breaking terms that the number of parameters increases to those displayed in table 2.2. Using the minimization conditions of the scalar potential reduces the parameters by $|\mu|$ and m_3^2 that can be expressed in terms of $m_{H_u}^2, m_{H_d}^2$ and $\tan\beta$.

Through mSUGRA we introduce the unification of the remaining SUSY breaking parameters. The gaugino masses are unified to $m_{1/2}$ which determines the masses of the neutralinos, charginos and gluinos at leading order. The SUSY breaking trilinear couplings are unified to A_0 and the ratio of the vacuum expectations values remains as a dimensionless input parameter.

m_0 finally unifies the remaining scalar mass terms for the squarks, sleptons and Higgs. $|\mu|$ and m_3^2 can be determined in terms of m_0 so that only the sign of μ has

to be set.

The complete set of input parameters is reduced to $m_0, m_{1/2}, A_0, tan\beta$ and $sgn(\mu)$.

2.3 The NMSSM

In the last section we described the μ-problem that refers to a cancellation of the SUSY respecting parameter μ with the SUSY breaking parameters $m^2_{H_u}$ and $m^2_{H_d}$. As this cancellation seems to have no motivation one attempt is to replace the parameter μ by an additional gauge-singlet chiral supermultiplet that only couples to itself and the Higgs. In this case the μ term will be generated by the vacuum expectation value of the singlet. One calls this the Next to Minimal Supersymmetric extension of the Standard Model, NMSSM. The conventions and computations in this section follow the report "The Next-to-Minimal Supersymmetric Standard Model" by U.Ellwanger, C. Hugonie and A.M. Teixeira [19].

The NMSSM now appears to have a richer phenomenology due to three additional particles and provides additional contributions to increase the lightest Higgs mass. The additional supermultiplet results in two scalar bosons, a CP-even Higgs (h_3) and a CP-odd Higgs (A_2), and one fermion, a fifth neutralino (χ^0_5).

To insert this supermultiplet into our Lagrangian we start again with the superpotential. From the MSSM we are familiar with the following superpotential that contains the Yukawa coupling between Higgs and quarks or leptons and the "μ term", the supersymmetric mass term of the Higgs.

$$W_{MSSM} = \mathbf{h_u}\hat{H}_u\hat{Q}\hat{U}^C_R - \mathbf{h_d}\hat{H}_d\hat{Q}\hat{D}^C_R - \mathbf{h_e}\hat{H}_d\hat{L}\hat{E}^C_R + \mu\hat{H}_u\hat{H}_d \tag{2.22}$$

The most general potential including the new gauge singlet is

$$W_{NMSSM} = W_{MSSM} + \lambda\hat{S}\hat{H}_u\hat{H}_d + \xi_F\hat{S} + \frac{1}{2}\mu'\hat{S}^2 + \frac{1}{3}\kappa\hat{S}^3 \tag{2.23}$$

where we have introduced four new parameters. λ and κ are dimensionless Yukawa couplings that couple the singlet to itself and the Higgs bosons. The term including μ' is the supersymmetric mass term for the singlet, comparable to the μ term that we know for the Higgs boson. Finally there is the tadpole term that is parametrized by ξ_F. In a global supersymmetry it can be removed by a constant shift of the singlet. Comparing the μ-term in equation 2.22 with the λ-term in equation 2.23 we observe that we are now able to generate an effective μ-term as soon as S acquires a non vanishing vev.

Given that the masses of the Standard Model particles and their partners are not degenerat, we have to introduce supersymmetry breaking parameters as for the MSSM. Apart from the appearance of a fifth neutralino in the gaugino sector, the modifications with respect to the MSSM only appear in the scalar sector.

In the following we focus on the scalar potential and list only the Higgs and singlet related terms. Starting again with the soft terms known from the MSSM, $\mathcal{L}^{MSSM}_{soft,Higgs}$, we find the following contributions for the complex scalar fields:

	MSSM	NMSSM
dimensionfull SUSY parameters	μ	ξ_F, μ'
(s.br.)	$m_3^2 (\equiv B\mu)$	$\xi_S, m_S'^2 (\equiv B'\mu')$
Higgs and singlet masses (s.br.)	$m_{H_u}^2, m_{H_d}^2$	m_S^2
Yukawa, trilinear couplings	$\mathbf{h_u}, \mathbf{h_d}, \mathbf{h_e}$	λ, κ
Trilinear couplings (s.br.)	$\mathbf{A_u}, \mathbf{A_d}, \mathbf{A_e}$	A_λ, A_κ
squark and slepton masses (s.br.)	$\mathbf{m_Q^2}, \mathbf{m_U^2}, \mathbf{m_D^2}, \mathbf{m_L^2}, \mathbf{m_E^2}$	
gaugino masses	M_1, M_2, M_3	

Table 2.3: Supersymmetric parameters of the NMSSM. The right column displays the parameters that enter in addition to the MSSM parameters.

$$\begin{aligned} -\mathcal{L}_{soft,Higgs}^{MSSM} =& m_{H_u}^2 |H_u|^2 + m_{H_d}^2 |H_d|^2 + (m_3^2 H_u H_d + h.c.)^1 \\ -\mathcal{L}_{soft}^{NMSSM} =& m_S^2 |S|^2 + \left(\lambda A_\lambda H_u H_d S + \frac{1}{3}\kappa A_\kappa S^3 + \frac{1}{2} m_S'^2 S^2 + h.c.\right)^1 \end{aligned} \tag{2.24}$$

Table 2.3 shows an overview of all parameters that we already know from the MSSM and those that are introduced in addition for the NMSSM. For the sake of completeness ξ_F is listed too.

2.3.1 The NMSSM Higgs Sector

Starting with the general form of the Lagrangian defined in the last section we will use some constraints and redefinitions to reduce the number of free parameters and bring them into a more convenient form.

1. The main motivation for the introduction of the NMSSM is the μ problem where the mass parameter μ has to cancel with SUSY breaking parameters although it arises from a SUSY respecting term(see section 2.2.3). Now that we have introduced the gauge singlet we can merge two terms of the superpotential:

$$W_{NMSSM} \supset (\mu + \lambda \hat{S}) \hat{H}_u \hat{H}_d \tag{2.25}$$

   Now we can generate an effective μ-term with the vev of the singlet while the parameter μ - which still has no reason to be of the order of the SUSY breaking scale - can be set to zero. Going one step further we can ask the superpotential to be scale invariant. Therefore we have to eliminate the remaining dimensionfull parameter μ' to zero. In contrast to the MSSM μ term it is possible

[1] One often finds the alternative definition: $m_3^2 = B\mu, m_S'^2 = B'\mu'$

to set μ' by setting it to zero as it is not determined by other parameters. By now we have suppressed the parameters μ, μ' and ξ_F. Following this attempt it is sensible to eliminate the corresponding SUSY breaking terms by setting $m_3^2 = m_S^2 = \xi_S = 0$.

By doing so we have not only made our potential scale independent but we have also introduced a new $\mathbb{Z}_3$-symmetry. Multiplying all chiral superfields with a factor $e^{i2/3\pi}$ leaves the Lagrangian now invariant.

2. In a second step we will use the minimization conditions of the vacuum expectation values to replace $m_{H_u}^2, m_{H_d}^2$ and m_S^2. The scalar NMSSM Higgs potential, including the soft SUSY breaking terms, reads:

$$
\begin{aligned}
V_{Higgs} = &\left|\lambda(H_u^+ H_d^- - H_u^0 H_d^0) + \kappa S^2\right|^2 && (2.26)\\
&+ \left(m_{H_u}^2 + |\lambda S|^2\right)\left(\left|H_u^0\right|^2 + \left|H_u^+\right|^2\right) && (2.27)\\
&+ \left(m_{H_d}^2 + |\lambda S|^2\right)\left(\left|H_d^0\right|^2 + \left|H_d^-\right|^2\right) && (2.28)\\
&+ \frac{g_1^2 + g_2^2}{8}\left(\left|H_u^0\right|^2 + \left|H_u^+\right|^2 - \left|H_d^0\right|^2 - \left|H_d^-\right|^2\right)^2 && (2.29)\\
&+ \frac{g_2^2}{2}\left|H_u^+ H_d^{0*} + H_u^0 H_d^{-*}\right|^2 + m_S^2 |S|^2 && (2.30)\\
&+ \left(\lambda A_\lambda (H_u^+ H_d^- - H_u^0 H_d^0) S + \frac{1}{3}\kappa A_\kappa S^3 + h.c.\right) && (2.31)
\end{aligned}
$$

When we now assume that we are in the minimum of the potential, the partial derivative of the potential with respect to H_u^0 has to be equal to zero. Therefore we expand the fields with non vanishing vevs (H_u^0, H_d^0, S) around their vevs:

$$
H_u^0 = v_u + \frac{H_{u,R}^0 + iH_{u,I}^0}{\sqrt{2}}, \quad H_d^0 = v_d + \frac{H_{d,R}^0 + iH_{d,I}^0}{\sqrt{2}}, \quad S = s + \frac{S_R + iS_I}{\sqrt{2}} \tag{2.32}
$$

Now we can take the partial derivative and evaluate this expression at the minimum, where the charged fields vanish as electromagnetism is unbroken.

$$
\begin{aligned}
0 = \left.\frac{\partial V_{Higgs}}{\partial H_u^0}\right|_{\substack{H_u^0 = v_u \\ H_d^0 = v_d \\ S = s}} &= \left(m_{H_u}^2 + \lambda^2 s^2\right) v_u + \frac{g^2}{4}\cdot 2(v_u^2 - v_d^2) v_u && (2.33)\\
&\quad - \lambda v_d(\kappa s^2 - \lambda v_u v_d) - \lambda A_\lambda v_d s && (2.34)\\
&= v_u\left(m_{H_u}^2 + \lambda^2 s^2 + \lambda^2 v_d^2 + \frac{g^2}{2}(v_u^2 - v_d^2)\right) && (2.35)\\
&\quad - v_d \lambda s(\kappa s + A_\lambda) && (2.36)
\end{aligned}
$$

As indicated for equation 2.23 we now replace every occurance of s by an effective μ parameter $\mu_{eff} = \lambda s$. Applying the same procedure to H_d^0 and S

leaves us with three equations that can now be used to express m_{H_u}, m_{H_d} and m_S in terms of v_u, v_d and μ_{eff}.

$$m_{H_u}^2 = -\mu_{eff}^2 - \lambda^2 v_d^2 + \frac{g^2}{2}(v_d^2 - v_u^2) + v_d/v_u \mu_{eff}(\frac{\kappa}{\lambda}\mu_{eff} + A_\lambda) \tag{2.37}$$

$$m_{H_d}^2 = -\mu_{eff}^2 - \lambda^2 v_u^2 + \frac{g^2}{2}(v_u^2 - v_d^2) + v_u/v_d \mu_{eff}(\frac{\kappa}{\lambda}\mu_{eff} + A_\lambda) \tag{2.38}$$

$$m_s^2 = -\frac{\kappa}{\lambda}A_\kappa \mu_{eff} - 2\frac{\kappa^2}{\lambda^2}\mu_{eff}^2 - \lambda^2(v_u^2 + v_d^2) + 2\lambda\kappa v_u v_d + \lambda^2 v_u v_d A_\lambda/\mu_{eff} \tag{2.39}$$

Finally we know that v_u and v_d can be replaced by the known mass of the Z-Boson and $\tan\beta$ the ratio of the Higgs vacuum expectation values that we know from the MSSM.

$$\left.\begin{array}{l} \tan\beta = \frac{v_u}{v_d} \\ m_z^2 = v^2 g^2 = (v_u^2 + v_d^2)\frac{g_1^2+g_2^2}{2} \end{array}\right\} \quad \begin{array}{l} v_u = v\sin\beta = \frac{m_z}{g}\sin\beta \\ v_d = v\cos\beta = \frac{m_z}{g}\cos\beta \end{array} \tag{2.40}$$

Now we are able to express $m_{H_u}^2, m_{H_u}^2$ and m_S^2 in terms of $\mu_{eff}, \tan\beta$ and m_Z, which are more familiar and hence more convenient as input parameters for our model. The obtained results will now be used to determine the Higgs masses.

2.3.2 The Higgs Mass

Considering the potential in section 2.3.1 we can derive an expressions for the Higgs mass matrices. Distinguishing between CP-even and CP-odd bosons we call the matrix for the real scalar fields M_S and the one for the imaginary part M_P. For M_S we set the basis to $(H_{d,R}^0, H_{u,R}^0, S_R^0)$. As an example we start with the term $M_{S,22}^2$. The only contributions from the Higgs potential that can contain terms with $(H_{u,R}^0)^2$ and no other field come from 2.26, 2.27 and 2.29. Collectings these terms we find:

$$M_{S,22}^2/2 = \frac{\lambda^2 v_d^2}{2} + \frac{1}{2}\left(m_{H_u}^2 + |\lambda s|^2\right) + \frac{g^2}{4}\left(3v_u^2 - v_d^2\right) \tag{2.41}$$

Replacing $m_{H_u}^2$ with equation 2.37 and using the relation 2.40 results in:

$$M_{S,22}^2 = m_Z^2 \sin^2\beta + \frac{1}{\tan\beta}\mu_{eff}\left(\frac{\kappa}{\lambda}\mu_{eff} + A_\lambda\right) \tag{2.42}$$

The remaining diagonal entries of the CP even mass matrix are:

$$M_{S,11}^2 = m_Z^2 \cos^2\beta + \tan\beta\mu_{eff}\left(\frac{\kappa}{\lambda}\mu_{eff} + A_\lambda\right) \tag{2.43}$$

$$M_{S,33}^2 = \lambda^2 \frac{A_\lambda m_Z^2}{2g^2\mu_{eff}}\sin 2\beta + \frac{\kappa}{\lambda}\mu_{eff}(A_\kappa + 4\frac{\kappa}{\lambda}\mu_{eff}) \tag{2.44}$$

For the off diagonal entries one finds:

$$M^2_{S,12} = \left(2\frac{\lambda^2}{g^2} - 1\right) m_Z^2 \sin\beta\cos\beta - \mu_{eff}\left(A_\lambda + \frac{\kappa}{\lambda}\mu_{eff}\right) \tag{2.45}$$

$$M^2_{S,13} = \lambda\frac{m_Z}{g}\left(2\mu_{eff}\cos\beta - \left(A_\lambda + 2\frac{\kappa}{\lambda}\mu_{eff}\right)\sin\beta\right) \tag{2.46}$$

$$M^2_{S,23} = \lambda\frac{m_Z}{g}\left(2\mu_{eff}\sin\beta - \left(A_\lambda + 2\frac{\kappa}{\lambda}\mu_{eff}\right)\cos\beta\right) \tag{2.47}$$

Although the masses of the bosons are the eigenvalues of the matrix and can not be deduced directly from the elements of the matrix, we can already infer some informations about the mass dependence on the additional NMSSM parameters.

The trilinear singlet coupling A_κ only appears in the diagonal entry of the singlet and will therefore only have a very small direct impact on the other Higgs masses. The selfcoupling of the singlet exclusively appears in the fraction κ/λ multiplied by μ_{eff}. This shows a strong correlation between the two parameters and a way the selfcoupling can enter indirectly. Also the mixing entries with the singlet are multiplied with λ as it is the coupling between the singlet and the Higgs sector. A_λ appears mainly in sums with κ/λ which hints at a correlation.

When one rotates the submatrix for the Higgs bosons by the angle β, the upper limit of the lightest Higgs mass becomes

$$m_Z^2\left(\cos^2 2\beta + \frac{\lambda^2}{g^2}\sin^2 2\beta\right). \tag{2.48}$$

The possible mass range is increased with respect to the MSSM if $\lambda > g$. This allows for smaller loop corrections and therefore smaller stop quark masses and smaller symmetry breaking. However this can only produce an actual effect if $\tan\beta$ is rather small.

For the CP odd bosons one can observe similar characteristics concerning κ, A_λ and A_κ.

$$M^2_{P,11} = 2\frac{\mu_{eff}(A_\lambda + \frac{\kappa}{\lambda}\mu_{eff})}{\sin 2\beta} \tag{2.49}$$

$$M^2_{P,22} = \lambda^2\left(A_\lambda + 4\frac{\kappa}{\lambda}\mu_{eff}\right)\frac{m_Z^2\sin\beta\cos\beta}{g^2\mu_{eff}} - 3\frac{\kappa}{\lambda}A_\kappa\mu_{eff} \tag{2.50}$$

$$M^2_{P,12} = \lambda^2\left(A_\lambda - 2\frac{\kappa}{\lambda}\mu_{eff}\right)\frac{m_Z}{g} \tag{2.51}$$

2.3.3 The Semi Constrained NMSSM

In the MSSM we drastically reduced the number of input parameters by mSUGRA, that introduces a unification at the GUT scale. In the same way we construct the semi constrained NMSSM. Similar to the unification conditions in mSUGRA we introduce the unification parameters $m_0, m_{1/2}$ and A_0.

m_0 is the mass of the scalar sleptons and squarks at the GUT scale. In contrast to the familiar mSUGRA model $m^2_{H_u}$ and $m^2_{H_d}$ don't take the value of m_0 at the GUT scale as they are already fully constrained by equation 2.37 and 2.38.

$m_{1/2}$ is the mass of the gauginos at the GUT scale. It unifies M_1, M_2 and M_3. Their values at the SUSY scale can be derived using the renormalization group equations (RGE).

A_0 is the unified trilinear coupling. It unifies $\mathbf{A_u}, \mathbf{A_d}$, and $\mathbf{A_e}$.

Taking into account all unifications, the number of additional input parameters with respect to the Standard Model from table 2.3 has reduced to $m_0, m_{1/2}, A_0, \tan\beta, \mu_{eff}, \lambda, \kappa, A_\lambda, A_\kappa$.

Compared to mSUGRA we can now set μ_{eff} and the additional parameters $\lambda, \kappa, A_\lambda$ and A_κ appear. These appear due to the additional singlet and the fact that $m^2_{H_u}$ and $m^2_{H_d}$ are not unified at the GUT scale. In this case - the constrained NMSSM - κ and μ_{eff} are no free parameters but can be computed from the minimization equations of the scalar potential that are otherwise used to determine $m^2_{H_u}$ and $m^2_{H_d}$.

2.3.4 RGEs

For an actual implementation of the model we have to specify the scale at which the input parameters are given. For those input parameters that are supposed to be a unified quantity at the GUT scale, namely $m_0, m_{1/2}$ and A_0 the GUT scale is an obvious choice. In order to offer the possibility to unify A_λ, A_κ with A_0 it is convenient to set them at the GUT scale too.
We have seen that $\tan\beta$ and m_Z can replace the Higgs vacuum expectation values v_u and v_d. Therefore $\tan\beta$ has to be defined at the electroweak scale. λ, κ and μ_{eff} are set at the SUSY breaking scale which is set to 1000 GeV. After setting the input parameters at a special scale, we use the RGEs to determine their value at the electroweak scale as suggested by Ref. [20].

In order to understand the behaviour of the additional NMSSM parameters at different scales, we take a look at their scale dependence. The scale dependence is parametrized by $t = \ln Q$. The renormalization group equations for the couplings are

$$16\pi^2 \frac{d\lambda^2}{dt} = \lambda^2(3h_t^2 + 3h_b^2 + h_\tau^2 + 4\lambda^2 + 2\kappa^2 - g_1^2 - 3g_2^2) \tag{2.52}$$

$$16\pi^2 \frac{d\kappa^2}{dt} = \kappa^2(6\lambda^2 + 6\kappa^2). \tag{2.53}$$

The RGEs are given for the square of the coupling. Therefore we can only make statements about their absolute value. For small values of λ the scale dependence is dominated by the top Yukawa coupling and grows with t. For higher values of

λ the coupling itself leads to a stronger increase until it reaches values bigger then 1 and is no longer weakly coupled. This means that the coupling can no longer be described by perturbation theory. If this happens before the GUT scale the model will be excluded.

The running of κ depends at leading order only on λ and itself. As both contributions are positive, κ will always increase exponentially with the scale.

$$16\pi^2 \frac{dA_\lambda}{dt} = 4\lambda^2 A_\lambda + 3h_t^2 A_t + 3h_b^2 A_b + h_\tau^2 A_\tau + 2\kappa^2 A_\kappa + g1^2 M_1 + 3g_2^2 M_2 \tag{2.54}$$

$$16\pi^2 \frac{dA_\kappa}{dt} = 6\kappa^2 A_\kappa + 6\lambda^2 A_\lambda \tag{2.55}$$

The scale dependence of A_λ depends on the sign of A_t and its ratio to the gaugino masses and A_κ through A_λ on the same variables.

For further analysis of the spectrum at the electroweak scale it is crucial to know how the known MSSM parameter are influenced by the additional NMSSM parameters.

Leading order contributions from λ appear in the RGEs of h_t, h_b, h_τ. Additional contributions from λ in combination with A_λ appear in the RGEs of A_t, A_b, A_τ, $m_{H_u}^2, m_{H_d}^2$. κ and A_κ appear in the same RGEs only in next to leading order terms.

$$16\pi^2 \frac{dh_t^2}{dt} = h_t^2(6h_t^2 + h_b^2 + \lambda^2 - \frac{13}{9}g_1^2 - 3g_2^2 - \frac{16}{3}g_3^2) \tag{2.56}$$

$$16\pi^2 \frac{dA_t}{dt} = 6h_t^2 A_t + h_b^2 A_b + \lambda^2 A_\lambda + \frac{13}{9}g_1^2 M_1 + 3g_2^2 M_2 + \frac{16}{3}g_3^2 M_3 \tag{2.57}$$

$$32\pi^2 \frac{d\mu}{dt} = \mu(3h_t^2 + 3h_b^2 + h_\tau^2 + 2\lambda^2 - g_1^2 - 3g_2^2) \tag{2.58}$$

The top Yukawa coupling decreases with t due to the large negative contribution of the SU(3) coupling. As λ^2 enters with a positive sign, it decreases the gradient of the running. As the Yukawa coupling is fixed by the top mass at the electroweak scale, this leads to a higher value for h_t^2 at the GUT scale compared to an MSSM scenario.

The trilinear coupling depends on too many arbitrary input parameters to make any prediction about the influence of A_λ.

The absolute value of μ will increases with t because of the combined effect of top, bottom and tau Yukawa coupling. The additional λ term increases the scale dependence and leads to a steeper incline. This effect is in accordance with the enhanced top Yukawa coupling.

The last RGE we consider is that of $m_{H_u}^2$. Therefore we define first the two

quantities

$$M_t^2 = m_{Q_3}^2 + m_{U_3}^2 + m_{H_u}^2 + A_t^2 \tag{2.59}$$
$$M_\lambda^2 = m_{H_u}^2 + m_{H_d}^2 + m_S^2 + A_\lambda^2. \tag{2.60}$$

The scale dependence of $m_{H_u}^2$ can now be written as

$$16\pi^2 \frac{dm_{H_u}^2}{dt} = 3h_t^2 M_t^2 + \lambda^2 M_\lambda^2 - g_1^2 M_1^2 - 3g_2^2 M_2^2. \tag{2.61}$$

The influence of the additional NMSSM parameters on the RGEs and the behaviour of the Higgs masses at tree level help us to understand the spectrum of the NMSSM. A key observable for physics beyond the SM is the amount of dark matter in the universe that is closely connected to the masses of the sparticles. Therefore we will now discuss how special mass configurations can lead to the correct relic density.

2.4 Dark Matter Annihilation Channels in SUSY

In the early universe dark matter has been produced in thermal equilibrium assuming a dark matter model with weakly interacting particles (WIMP) as in supersymmetry. In equilibrium the number density follows the Boltzmann equation

$$\frac{dn_\chi}{dt} + 3Hn_\chi = - < \sigma_A v >_T [n_\chi^2 - n_{\chi,eq}^2] \tag{2.62}$$

The Hubble constant H accounts for the expansion of the universe, $< \sigma_A v >_T$ is the thermally averaged annihilation cross section and the term in brackets adjusts the creation and annihilation cross section to generate the number density in equilibrium.

The expansion of the universe causes a drop in the temperature. When the temperature becomes smaller than the mass of the WIMP, the pair creation of the dark matter needs particles from the tail of the velocity distribution. Therefore the number density decreases exponentially. At some point the density of dark matter particles is so low, that the annihilation cross section becomes smaller than the effect caused by the expansion of the univers. At that point the freeze out occurs as the dark matter can no longer annihilate.

The amount of dark matter in the universe today depends therefore on the annihilation cross section of dark matter before the freeze out. To generate a small relic density it is crucial to find an annihilation process with a sufficiently high cross section. In the following we will discuss typical annihilation channels for dark matter in supersymmetric models.

In supersymmetry the dark matter candidate is the LSP, the lightest supersymmetric particle, as it can not decay any further into supersymmetric or Standard Model particles. As it has to be "dark", which means not having an electric charge,

the only possible candidates are neutralinos, sneutrinos and gravitinos. The MSSM sneutrinos have already been ruled out by experiments, so we will focus on the lightest neutralino as a dark matter candidate [15] and discuss its annihilation channels.

h-funnel

h-funnel means that two LSP annihilate into a Higgs boson which consequently decays into a particle and an antiparticle, mostly $b\bar{b}$, as shown in Fig. 2.2. The cross section for this process and therefore the annihilation efficiency is highest if the process is on shell. Taking into account that the particles in the early universe move with non negligible velocity v we get the following mass relation for Higgs and LSP in CMS for the on shell case:

$$m_h^2 = (p_1 + p_2)^2 = (2E_{1/2})^2 = 4(m_{\chi_1^0}^2 + \vec{p}^2) = 4\gamma^2 m_{\chi_1^0}^2 \tag{2.63}$$

why including v/c, isn't that correction small?

$$m_{\chi_1^0} = \frac{m_h}{2}\sqrt{1 - \frac{v^2}{c^2}} \tag{2.64}$$

As the mass of the Higgs is known, this sets the mass of the LSP. In the usual case of a neutralino LSP, the LSP is usually "bino-like" and depends strongly on M_1 respectively $m_{1/2}$ in SUGRA like Models. Therefore investigating a likelihood map of for SUGRA like models, one can easily identify the Higgs funnel region in a projection on the m_0-$m_{1/2}$-plane.

A-funnel

The concept of the A-funnel region is similar to that of the h-funnel. Differences arise due to the width of the A boson at the order of 40 GeV and therefore about 4 orders of magnitude bigger than that of the SM Higgs. Even if we fix the mass of the LSP to $m_{\chi_1^0} = 740.9GeV$, we find the correct relic density e.g. for $m_A = 1497.9\,\text{GeV}$ as well as $m_A = 1505.3\,\text{GeV}$ which shows that it is not necessary to hit the pole. Furthermore the mass of A is not fixed by current experiments. Thus there is a wider region in the parameter space of mSUGRA that corresponds to this region.

Co-annihilation region

Co-annihilation regions can appear for sleptons [21], squarks [22] and charginos [23]. For this type of annihilation channels the mass of the next-to-lightest supersymmetric particle has to be close to mass of the LSP. The mass difference can only be of the order of a few percent or less. Otherwise this particle would decay into its SM partner and the LSP. If the masses are nearly degenerate, this decay is suppressed

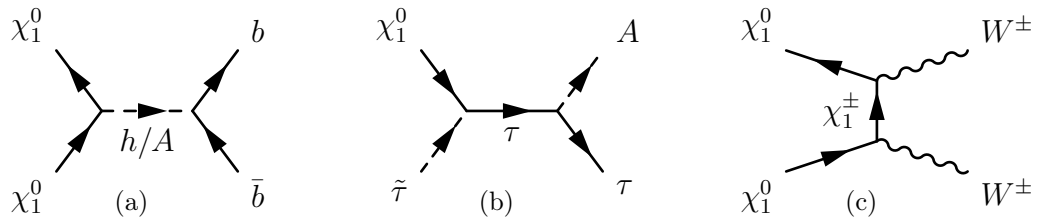

Figure 2.2: Dark matter annihilation processes for the funnel region (a), the $\tilde{\tau}$-co-annihilation region (b) and the focus point (c).

by the phase space. In the example of a $\tilde{\tau}$-co-annihilation [21] the annihilation process is an s-channel diagram. $\tilde{\tau}$ and the LSP annihilate via a τ lepton into a τ and a pseudo scalar Higgs. In this case the LSP can have a large Higgsino component as the coupling is determined by the Yukawa coupling that is enhanced sufficiently only for stau and the stop squark. For co annihilation with the lightest stop squark the lightest stop mass should be in the range of 1- 1.05 times the LSP mass. [24]

Focus point region

The focus point region [25] is defined by gaugino and Higgsino masses at the electro weak scale while squarks and sleptons become heavy. This region is consequently determined by large m_0 and small $m_{1/2}$. The focussing enters through the requirement that the electroweak potential is insensitive to small changes of the SUSY breaking parameters. The correct relic density can be be provided by an LSP with a non trivial Higgsino or wino component and a mass around the electroweak scale. μ is very small to generate the according mixing. The annihilation then goes via a t-channel chargino into two W bosons.

the well-tempered region is missing, or not?

3 Measurements

Among the data, that we use for the fit, we first of all choose those experiments that made it necessary to search for new physics. Dark matter for example doesn't exist in the SM and supersymmetry is supposed to introduce a particle that will provide a dark matter candidate. The exact Higgs mass is neither predicted by the Standard Model but when we set the input parameters for the NMSSM the masses of the three CP even Higgs bosons will be fixed and one of them will have to be consistent with the discovered scalar.

To test the validity of the tested model we also use precision measurements that will be sensitive to new particles e.g. through loop contributions. We include the anomalous magnetic moment, B-Physics observables and results from experiments in the electroweak sector. Starting with the Higgs mass the impacts of the different measurements are now explained in detail. The given statistical and systematic errors are taken from the official papers. The theory errors arise from uncertainties on the supersymmetry calculations. For the Higgs mass, the relic density, the anomalous magnetic moment and the branching ratio $BR(B_s^0 \to \mu^+\mu^-)$ the theoretical errors on the SUSY calculations have been estimated in the SFitter paper [26].

3.1 Higgs Mass and Couplings

$m_h = (126.0 \pm 0.4\ _{stat} \pm 0.4\ _{syst} \pm 3.0\ _{theo})\,\text{GeV} \qquad (ATLAS[4] + theo.\,uncert.)$

So far the Higgs boson is the only detected elementary scalar particle. Its mass measurements by ATLAS and CMS are compatible within the statistical and systematic errors. As the theoretical error of the SUSY calculations is more than five times bigger than the combined statistical and systematic error, a combination of both measurements would not change the results significantly.

The main production channel for the Higgs at the LHC is gluon fusion through a top loop followed by weak boson fusion and the associated Higgs production. A produced Higgs of about 125 GeV decays mainly into a $b\bar{b}$ pair that forms jets, which are indistinguishable from the background for gluon fusion. The same applies for a decay into gluons or $c\bar{c}$. For Higgs production associated with a W or Z boson and weak boson fusion, it is possible to distinguish the decay into $b\bar{b}$ from backgrounds like $q\bar{q} \to Zg^* \to Zb\bar{b}$ [27], but the resolution remains weak. Finally the mass of the Higgs has been reconstructed in the decay channels $H \to ZZ \to 4l$ and $H \to \gamma\gamma$ that have a smaller cross section but a better signal to background ratio and mass resolution.

After the discovery of the Higgs bosons these channels remain an important source

for further informations. The measurement of the mass has been improved due to more accumulated statistics and the Yukawa couplings can be measured through a wide variety of different production and decay channels [28].

In the context of supersymmetry the detected boson is just one of many scalars. In the MSSM there are two CP even Higgs bosons, in the NMSSM even three. In the MSSM the tree level mass of the lightest Higgs is limited by the mass of the Z boson (sec. 2.2.2) which is in tension with the measurement. A correct mass can either be obtained by loop corrections from heavy stop quarks or by choosing a heavier Higgs to be the one at 126 GeV. In the NMSSM (sec. 2.3.2) the lightest Higgs mass on tree level can also be slightly increased if the ratio $\frac{\lambda^2}{g^2}$ is bigger than 1. In this study we assume the lightest Higgs to be Standard Model like which leads to high masses of the stop quark in regions that are compatible with the experimental data.

3.2 The Relic Density

$\Omega h^2 = 0.1187 \pm 0.0017\ _{stat} \pm 0.0120\ _{theo} \qquad (Planck[2] + theo.\,uncert.)$

The amount of dark matter in the whole universe is determined by methods like gravitational lensing and cosmic microwave background (CMB).

Astronomical measurements like the observation of quasars lead to the conclusion that dark matter is made up of cold particles. In the early universe mass was distributed in a homogeneous way. Photons and baryons were coupled into a plasma, a perfect fluid, due to rapid scattering. The inflationary seeds of the universe's structure were quantum overdensities that created potential gravitational wells. While the gravitational force pulled the fluid into the centre of these fluctuations the photon pressure leads to a rejection forming so called acoustic oscillations. The combined effects of gravitation and photon pressure lead to periodic compression (overdensities) and rarefications (underdensities). Due to its expansion, the universe cooled down so that atoms could form from free electrons and protons and the universe became transparent for photons. The so called freeze out lead to a cut off in in the oscillations and the freed photons are nowadays observed as CMB. The radiation is isotropic at a level of 10^{-5} and its spectrum corresponds to that of a black body with a temperature of 2.725 K [29].

The amount of dark matter in the universe is determined from the small temperature anisotropies of the CMB [2]. One expands them in terms of the normalized spherical harmonics:

$$\frac{\delta T}{T_0}(\theta, \phi) = \sum_{l=0}^{+\infty} \sum_{m=-l}^{+l} a_{lm} Y_{lm}(\theta, \phi) \tag{3.1}$$

The contained informations can be extracted by considering the variance

$$C_l \equiv < |a_{lm}|^2 > = \frac{1}{2l+1} \sum_{m=-l}^{l} |a_{lm}|^2 \tag{3.2}$$

multiplied by $l(l+1)/2\pi$. $l = 0$ corresponds to a monopole and $l = 1$ to a dipole moment. The dipole moment is caused by the motion of the solar system relative to the CMB. For $l \geq 2$ the variances carry information about the intrinsic anisotropy of the CMB. Higher values of l correspond to smaller angles and scales.

This spectrum can now be used to determine best-fit parameters for cosmological models and thereby the relic density.

The Wilkinson Microwave Anisotropy Probe (WMAP) data [30] lead to an amount of baryons and matter of

$$\Omega_b h^2 = 0.024 \pm 0.001 \quad \text{and} \quad \Omega_M h^2 = 0.14 \pm 0.02 \tag{3.3}$$

The relic density is obtained as the difference between total matter and baryonic matter.

The WMAP results have been combined amongst others with those obtained by ACBAR [31] and CBI [32] that studied smaller scales than WMAP. The combined measurement benefits from smaller uncertainties and results in[33]

$$\Omega_b h^2 = 0.0224 \pm 0.0009 \quad \text{and} \quad \Omega_M h^2 = 0.135^{+0.008}_{-0.009} \tag{3.4}$$

The latest results for the dark matter density are provided by the Planck collaboration [2]. The spacecraft that was collecting data from 2009 to 2013 measured radiation of the CMB in nine frequency bands. The combined results have been used to construct a full-sky map of the CMB from which the actual value for the dark matter density was obtained. To improve the reliability the Planck result has been combined with large scale polarization data from WMAP [34], results from the South Pole Telescope and the Atacama Cosmology Telescope [35], and baryon acoustic oscillation measurements (BAO) [36]. The higher angular resolution enables Planck to make more precise measurements on its own without encountering difficulties through combinations with other measurements.

3.3 The Anomalous Magnetic Moment

$a_\mu = (287 \pm 63\ _{exp} \pm 49\ _{SM} \pm 20\ _{theo}) \cdot 10^{-11} \qquad (Muon\, G-2[37], [3] + theo.\, uncert.)$

The magnetic moment of a particle is a quantity that determines the influence of an external magnetic field. The magnetic moment of a single particle is related to its spin, charge and mass by the Landé factor g.

$$\vec{\mu} = g\frac{e}{2m}\vec{s} \tag{3.5}$$

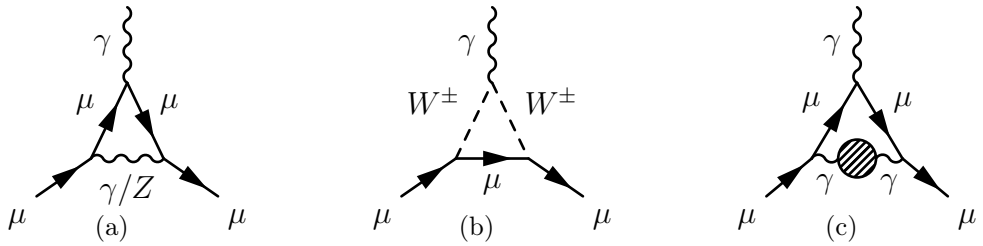

Figure 3.1: Standar Model loop corrections to the magnetic moment. From left to right: QED (a), EW (a,b) and hadronic (c) corrections.

The Dirac equation predicts $g = 2$ for spin-1/2 particles like the electron and the muon. QED, EW and hadronic loop corrections to this vertex (see feynmangraphs) lead to deviations from 2. These deviations from the Dirac prediction are quantified as the anomalous magnetic moment.

$$a = \frac{g-2}{2} \tag{3.6}$$

$$a_{SM} = (116591802 \pm 2_{QED+EW} \pm 42_{had,LO} \pm 26_{had,HO}) * 10^{-11} \tag{3.7}$$

While the electroweak corrections can be predicted with a high accuracy, the low order and high order hadronic corrections lead to an uncertainty of about $49 \cdot 10^{-11}$ when summed up quadratically.

Comparing the experimental value obtained by the Muon G-2 Collaboration [37] and the theoretical prediction for the Standard Model including electroweak and hadronic corrections leads to a discrepancy of 3.6 σ.

$$a_{exp} = (116592089 \pm 54 \pm 33) * 10^{-11} \tag{3.8}$$

$$\Delta a_\mu = a_{exp} - a_{SM} = (287 \pm 63 \pm 49) * 10^{-11} \tag{3.9}$$

Supersymmetry would add further loop corrections [38] which enlarge the value of a and could lead to a better agreement with data.

3.4 Other Observables

The following observables only have minor influence on the fit results. The experimental results are listed in table 3.1.

B-Physics

The rate $b \to s\gamma$ measures the flavour changing neutral current that is only possibly through a loop. It can be obtained from the measurement of $B \to X_s\gamma$ that has

Measurement	Value and error	
$BR(B \to X_s\gamma)$	$(3.55 \pm 0.24\ _{stat} \pm 0.09\ _{syst}) \cdot 10^{-4}$	[39]
$BR(B_s^0 \to \mu^+\mu^-)$	$(3.2 \pm 1.4\ _{stat} \pm 0.5\ _{syst} \pm 0.2\ _{theo}) \cdot 10^{-9}$	[42]
$BR(B^+ \to \tau^+\nu)$	$(1.41 \pm 0.43\ _{stat}) \cdot 10^{-4}$	[43]
Δm_{B^0}	$(0.510 \pm 0.004\ _{stat} \pm 0.003\ _{syst} \pm 0.400\ _{theo}) \cdot 10^{12}\,\hbar\mathrm{s}^{-1}$	[43]
$\Delta m_{B_s^0}$	$(17.69 \pm 0.08\ _{stat} \pm 7.00\ _{theo}) \cdot 10^{12}\,\hbar\mathrm{s}^{-1}$	[43]
$\Gamma_{Z\to Inv}$	$(-1.9 \pm 1.5\ _{stat} \pm 0.2\ _{theo})\,\mathrm{MeV}$	[44]
$\Gamma_{Z\to Higgs}$	$(6.5 \pm 2.3\ _{stat} \pm 1.0\ _{theo})\,\mathrm{MeV}$	[44]
m_t	$(173.5 \pm 0.6\ _{stat} \pm 0.8\ _{syst})\,\mathrm{GeV}$	[45]

Table 3.1: Data used for the fit including their systematic and statistical errors from the measurements and theoretical errors for SUSY calculations as far as they are considered.

been performed by BaBar, CLEO and Belle [39]. The combined value is displayed in Table 3.1. The bottom quark is converted through a loop containing a W and an up type quark into a strange quark and a photon that is necessary for momentum conservation. Recent NNLO calculations for the Standard Model predict a value of $(3.15 \pm 0.23) * 10^{-4}$ [40] and $(2.98 \pm 0.26) * 10^{-4}$ [41] for $E_\gamma > 1.6\,\mathrm{GeV}$. Supersymmetry introduces additional loop contributions including Higgsinos, winos, binos and gluinos. These contributions increase the value of the rate.

The decay $B_s^0 \to \mu^+\mu^-$ is as well only possible through a loop and receives additional contributions from SUSY particles. The measurement of the branching fraction has been performed by LHCb with their data from 2011 and 1012 [42].

The branching ratio $B^+ \to \tau^+ + \nu$ has been measured by BaBar and Belle [43]. The s-channel decay that goes through the W-boson for the Standard Model can get contributions from the charged Higgs boson.

$\Delta_{m_{B^0}}$ is a measure for the oscillation frequency of a $B - \bar{B}$-system. The HFAG average value [43] has been calculated from a large number of experiments. The most recent measurements have been carried out by LHCb, D0, BaBar and Belle.

The average value for the $B_s - \bar{B}_s$ mixing $\Delta_{m_{B_s^0}}$ has also been evaluated by the HFAG using the results from LHCb and CDF. The theoretical errors are estimated from the ones calculated in NMSSMTools. The main contributions come from uncertainties on CKM matrix elements and lattice QCD calculations.

Electroweak Precision Data

For the electroweak measurements the branching ratios of the Z-boson are taken into account. The decay of $Z \to \nu\bar{\nu}$ or more general Z to invisible receives additional contributions from the decay into the LSP $Z \to \chi_1^0 + \chi_1^0$. Therefore the value given

in table 3.1 is the difference between the measured value (499 MeV ± 1.5 MeV (fit using lepton universality) / 503 MeV ± 16 MeV (average)[44]) and the Standard Model prediction (500.9 MeV). The second branching ratio is the difference between the measured total decay width of the Z boson (2495.2 MeV ± 2.3 MeV [44]) and the SM prediction (2488.7 MeV). Additional contributions of the NMSSM with respect to the Standard Model can compensate for this difference. They will arise from the decay into Higgs bosons $Z \to h_i + A_j$ if the decay products are together lighter than the Z boson.

Top Quark Mass

Having a mass of about 175 GeV the top mass is so far the heaviest elementary particle. Due to its large mass it has a lifetime that is too short to form bound states which is unique for the quark sector. Instead it decays immediately into a W boson and a down type quark which then hadronize. The mass measurements [45] have been performed by ATLAS, CDF, CMS and D0. Due to its high mass and the corresponding Yukawa coupling of about 1 the top mass is an essential parameter for BSM physics. Appearing in loop contributions small changes in his mass can have big effects on observables. Therefore the top mass will later be used as a variable input parameter. At the same time the measurement of the top quark mass will be taken into account in the fit.

4 SFitter

4.1 Idea

The attempts to explain deviations from the Standard Model have result and continue to result in a huge amount of new theories. Each theory again results in different models and each model is characterized by a certain number of input parameters that can be chosen freely in a defined range.

This makes it necessary to develop efficient and flexible tools to compare the given data with the predictions of many models. SFitter is such a program. It is designed in a way that allows to implement arbitrary models and then do a fit over different input parameters to determine their likelihood and find best fitting points for the given data. SFitter has been used for the determination of supersymmetric parameters [9], including a bottom-up renormalization group analysis and experimental information on production rates [46], as well as Higgs coupling measurements [47] for MSSM scenarios.

The likelihood of a set of model parameters given experimental results is defined as the probability to measure these results if the model is true [10]. Both expressions are meant to be evaluated over the parameter space of the model.

$$L(mod|meas) = P(meas|mod) \tag{4.1}$$

To determine a probability one has to consider the errors on the measurement as well as the theoretical error from the prediction. The experimental errors are divided into systematic and statistical errors. For a small number of events the statistical error of a measurement is described by a Poisson distribution. If the number of events increases, the distribution approaches the limit of a Gaussian.

The systematic errors of a measurement arise for example from efficiencies in particle identification or calibration of jet and lepton energy scales. They can be described by a Gaussian as they are often determined from background processes that have a high number of events.

Therefore both experimental errors can in many cases be described by a Gaussian.

$$L(y) = e^{-\frac{(x-y)^2}{2\sigma^2}} \tag{4.2}$$

Theoretical errors often arise from higher order QCD effects in perturbation theory. It follows that the probability distribution does not peak around a central value but remains flat. Nevertheless we assume that perturbation theory is able to describe the prediction and so the uncertainty has to be limited. The theoretical

uncertainty is therefore described as a flat box-shaped error.

$$L(y) = \Theta(y - x_{min})\Theta(x_{max} - y) \tag{4.3}$$

To evaluate the likelihood of a measurement one has to combine the systematic, statistical and theoretical errors. As the convolution of two Gaussian results again in a Gaussian the systematic and the statistical uncertainties are combined by adding the standard deviations squared. To combine the Gaussian with the theoretical flat box-shaped error we have to determine the convoluted likelihood. It is given by

$$L(x) = \max_y \Theta(y - x_{min})\Theta(x_{max} - y) e^{-\frac{(x-y)^2}{2\sigma^2}} \tag{4.4}$$

$$= \max_{y[x_{min}, x_{max}]} e^{-\frac{(x-y)^2}{2\sigma^2}} \tag{4.5}$$

$$= \begin{cases} e^{-\frac{(x-x_{min})^2}{2\sigma^2}} & \text{for} \quad x < x_{min} \\ 1 & \text{for} \quad x[x_{min}, x_{max}] \\ e^{-\frac{(x-x_{max})^2}{2\sigma^2}} & \text{for} \quad x > x_{max} \end{cases} \tag{4.6}$$

The result is a Gaussian that has been cut at its peak to insert a flat distribution with the length of the theory error. The same is true for the combination of a Poisson distribution with a box shaped error. The combination of a Possion distribution with a Gaussian proceeds in the same way leading to the non trivial result

$$L(x) = \max_y \exp\left(-N + y \log N - \log y! - \frac{(x-y)^2}{2\sigma^2}\right). \tag{4.7}$$

This construction is called RFit scheme [48].

To combine different observables one has to multiply all involved likelihoods. Therefore it is numerically more stable to consider their logarithms that only have to be added. If we consider the log-likelihood in the limit of a Gaussian, the logarithm of the likelihood corresponds to the χ^2 value by

$$L(x) = e^{-\frac{x^2}{2\sigma^2}} = e^{-\frac{\chi^2}{2}} \Leftrightarrow \chi^2 = -2 \log L(x) \tag{4.8}$$

SFitter allows to include correlations between the measurements. The correlation is implemented by means of the symmetric correlation matrix C. For independent measurements the correlation matrix is simply diagonal. Generalizing the relation between the likelihood and χ^2 for correlated measurements in the RFit scheme replaces χ^2 by

$$-2 \log L = \vec{x} C \vec{x}^T \tag{4.9}$$

$\vec{x}$ represents all observables that are taken into account. Its components x_i are determined to be

$$x_i = \begin{cases} \frac{x_{meas,i}-x_{mod,i}+\sigma_{theo,i}}{\sigma_{exp,i}} & \text{for} \quad x_{meas,i} < x_{mod,i} - \sigma_{theo,i} \\ 0 & \text{for} \quad |x_{meas,i} - x_{mod,i}| < \sigma_{theo,i} \\ \frac{x_{meas,i}-x_{mod,i}-\sigma_{theo,i}}{\sigma_{exp,i}} & \text{for} \quad x_{meas,i} > x_{mod,i} + \sigma_{theo,i} \end{cases} \tag{4.10}$$

in order to reproduce χ^2 in the limit of uncorrelated measurements with Gaussian errors.

For this study correlations between the Higgs mass and the Higgs couplings are taken into account. All other measurements like $g-2$ are considered to be independent.

4.2 Bayesian vs. Frequentist

After calculating the likelihood for many points in the parameter space one has to project the result on a two dimensional plane to display it. Therefore exist two methods to project a multidimensional parameter space on a lower dimensional one.

Bayesian

Using the Bayes' theorem we can show that the likelihood is proportional to the probability that a model is true given the measurements.

$$P(mod|meas) = P(meas|mod)\frac{P(mod)}{P(meas)} = L(mod|meas)\frac{P(mod)}{P(meas)} \tag{4.11}$$

The likelihood can therefore be determined when we know the probability of the measurement, the probability of the model The probability of the measurement $P(meas)$ gives an normalization factor that has to ensure that $P(mod|meas)$ integrated over $P(meas)$ is normalized to unity.

The probability $P(mod)$ on the other hand implies a measure that depends on the choice of the model parameters. This choice is in principle arbitrary, but it introduces a prior that has to be taken into account. When we project the likelihood map on a lower dimensional map we have to integrate over the spare parameters taken into account the introduced prior.

In SFitter the integration is done by counting the number of times the Markov chains ends in one bin and weighted with the prior.

Frequentist

The frequentist method uses another approach. We assume a given likelihood of a n+1-dimensional parameter space $L(x_1, ..., x_n, y)$, that we want to reduce to a likelihood over a n-dimensional parameter space $L(x_1, ..., x_n)$. Instead of integrating over the spare parameter y, the higher dimensional map is projected on the lower

dimensional one by choosing the value of y that maximizes the probability. The new likelihood distribution is given by

$$L(x_1, ..., x_n) = \max_y L(x_1, ..., x_n, y). \tag{4.12}$$

One calls this a profile likelihood. In the present studies we use the frequentist method to avoid the influence of a prior of the Bayesian method.

4.3 Implementation

The fitter tries to maximize the likelihood in the given range of the input parameters using markov chains. In doing so for each selected point of the parameter space SFitter has to call the tools that calculate the observables which are compared to the data. One strength of SFitter is, that it keeps different tools well separated from each other, so that one can run them independently and use only those that one needs for a certain setup. A common SLHA-file enables the tools to communicate.

We will look at its two input files - one for the model and one for the data - to illustrate how this is working in detail.

In the modelfile one first specifies the model that one wants to use. This is necessary to reserve memory for the model specific input parameters.

Then one selects the tools that calculate observables like masses or the relic density from the input parameters. The tools have to be set in the right order so that consecutive programs can use the output of previous ones.

Next, different global preferences can be specified, e.g. the GUT-scale is set to $3 \cdot 10^{17}$ GeV and the CMS energy is set to 7 TeV.

After the tools, the fitter along with its settings has to be calibrated. Here we use markov chains with 200000 points and a flat prior.

Finally one has to set the input parameters of the model and the Standard Model values for some parameters like the top mass. These values can be fixed or a range can be given by the lowest and the highest value and a third value that sets the fineness of the grid for the fit.

For each point of the Markov chain the corresponding input parameters are written into the SLHA-file. The different tools know the address of the input parameters and fill the SLHA file with their results until the final observables are calculated. Their address again has to be given in the data file to relate the provided results of measurements and their errors with the predictions that are now stored in the SLHA file.

In the data file the measured values and their errors are set. Statistical and systematic errors enter as Gaussian errors while the theory errors enter flat. As described before this means that within the theory limits all values have the same probability while outside these limits the probability decreases as the Gaussian of the statistical and systematic errors.

4.4 Markov Chains

Before choosing a special fitting tool we have to know what we expect from the results. For instance one can do a scan over the whole parameter space by setting a grid. In this case one gets an overview over the whole space and a reasonable idea of the underlying structures. One problem for this method is that the time for the scans grows exponentially with the number of parameters. Even if we have only 4 input parameters and we want to increase the finesse for each by a factor of 5 the calculation time gets multiplied by $5^4 = 625$. Additionally such a scan will treat areas with small probability - in which we are not interested - the same way as areas with a high probability.

Another method is a fit that tries to find the point in the parameter space that describes the data best. This brings us already closer to what we want, as we are interested in parameter configurations that might actually be realised in nature, but this time we won't see the structure of the area around.

To solve this problem we use Markov Chains with different starting points. The concept of Markov Chains is, that the next step only depends on the current state of a system. The Markov Chain tries to find a point with higher likelihood following a proposal function for choosing the next point in parameter space. The proposal function is a Breit-Wigner distribution which means the closer another point in parameter space the more likely it is chosen as a next point of the chain.

This way the Markov chain searches for points in parameter space with higher probability. If it finds a better point the new point will be the starting point for the next search.

For each new calculation the fitter has to launch each of the tools that are necessary to calculate the spectrum and the observables. In the following we introduce the most importan tools available for SFitter.

4.5 Tools

SuSpect

SuSpect [52], a spectrum calculator for the MSSM has been used so far for mSUGRA and general MSSM studies. The running of the gauge couplings, the Yukawa couplings and the gaugino mass terms are calculated at 2-loop level. The Higgs masses are calculated at 1-loop level including leading contributions at 2-loop level. The remaining parameters are calculated at 1-loop level. While SuSpect2 was entirely fortran based, SuSpect3 has a C++ interface that makes it easier accessible.

SuSyHit

SuSyHit [53] is an interface between SuSpect, SDECAY and HDECAY. SDECAY calculates the widths and branching ratios for supersymmetric particles in the MSSM. HDECAY calculates the same observables for the Higgs bosons.

SUSY-POPE

SUSY-POPE (SUSY Precision Observables Precisely Evaluated) [54] is a mainly fortran based program that is used to calculate the partial decay widths of the Z boson, pole cross sections for e^+e^- collisions and asymmetry parameters for the SM and the MSSM.

4.5.1 NMSSMTools

NMSSMTools is a compilation of tools to calculate the Higgs and sparticle spectrum of the NMSSM including some extra observables like contributions to the anomalous magnetic moment. It contains the tools NMHDECAY [55], NMSPEC [56], NMGMSB [57] and NMSDECAY [58] written by Ulrich Ellwanger, John F. Gunion, Cyril Hugonie, C.-C. Jean-Louis and Ana M. Teixeira.

For the present studies we use NMSPEC and NMHDECAY. They calculate the masses of the Higgs and the sparticles, the decay widths and the couplings of the Higgs. In order to include NMSSMTools as tools in SFitter we had to split the program into independent parts. The so created tools are called NMSSMSPECTRUM, NMSSMDECAY, NMSSMEW, NMSSMGMU and NMSSMBPHYSICS. Furthermore we had to create interfaces for each program to connect the fortran based NMSSMtools with SFitter that is written in C++.

The fortran structure to store data is the common block. The common block allocates its data so that one can access them via "commonblock.variable". The interface can therefore fill the common block with the data from the SLHA file and overwrite the SLHA input after the computation with the new results that are stored in the common block.

The first tool that is launched is NMSSMSPECTRUM. After initializing the input it runs the RGEs to compute the values of the soft SUSY breaking parameters at the SUSY breaking scale. All couplings and soft terms are calculated at 2 loop level. If the computation is successful the program will continue computing the masses of the sfermions, the Higgs bosons, the gluinos, charginos and neutralinos. This includes the computation of the corresponding mixing matrices. They are e.g. necessary for the calculation of the additional contributions to the Z width due to decays into Higgs bosons. The calculation of the Higgs boson masses includes the full 1 loop corrections including pole masses and the 2-loop corrections that originate from top and bottom Yukawa couplings.

The next tool that originates from NMSSMTools is NMSSMDECAY. It calculates the total width and the branching ratios of the charged and the five neutral Higgs boson. The branching ratios are necessary to predict the cross sections for different channels used to determine the coupling of the Higgs. The predictions are made by HIGGSPROD. When we include HIGGSPROD the sequence of the programs becomes crucial. We use HDECAY to calculate the Standard Model branching ratios for a given Higgs mass. For the NMSSM there are three cp even Higgs bosons and hence three possible candidates. Therefore one has to specify in ToolHdecay.cxx and

in the modelfile (HIGGSPROD) which Higgs boson is supposed to be the Standard Model like. Now HDECAY fills the SLHA-file not only with the branching ratios for a Standard Model like Higgs but also with the MSSM branching ratios for those Higgs bosons that would appear in the MSSM. These have to be overwritten by NMSSMDECAY. Afterwards HIGGSPROD has all necessary informations to calculate the crosssections for the channels.

The other NMSSM tools can be called afterwards in arbitrary sequence.
NMSSMEW calculates the additional contributions to the Z width due to decays into Higgs bosons and the lightest neutralino which contributes to the partial decay width of Z into invisible.
NMSSMGMU calculates the NMSSM contributions to the anomalous magnetic moment of the muon up to 2-loop contributions.
NMSSMBPHYSICS calculates the branching ratios $b \to s\gamma, B_s^0 \to \mu^+\mu^-$ and $B^+ \to \tau^+ + \nu$ and the mass differences $\Delta_{m_{B^0}}$ and $\Delta_{m_{B_s^0}}$

4.5.2 MicrOMEGAs

MicrOMEGAs [59] is a program, that calculates dark matter properties like the relic density for a given model. The program itself has been included as a tool before for the MSSM and has been used in combination with SuSpect. Adding now the NMSSM produces library conflicts. As MSSM and NMSSM use different input parameters, the input depends on the chosen model. Hence we had to implement a new reading routine to fill the additional mixing matrix for the CP odd Higgs bosons and the bigger mixing matrices for the neutralinos and the CP even Higgs bosons.

Moreover in MicrOMEGAs exist two distinct directories MSSM and NMSSM that have their own libraries. Due to double assignment of some variables we can not load both libraries at the same time. In order to access MicrOMEGAs with the same tool independent of the model we have to implement dynamic loading of the libraries.

5 Constraining the NMSSM

In the previous chapters we have introduced the NMSSM. Starting with the simplest implementation of supersymmetry, we have motivated the introduction of an additional singlet and followed this path to the actual realisation in a semi constrained model with only few input parameters. The general NMSSM differs from the MSSM only by the introduction of an additional singlet. Therefore the parameter space of the MSSM is a subspace of the NMSSM parameter space and one can embed it by decoupling the additional singlet. In the same way mSUGRA is a subspace of the semi constrained NMSSM, as all constraints applied for the semi constrained model have also been applied to mSUGRA. mSUGRA can therefore be embedded into the larger parameter space of the semi constrained model. We illustrate this by considering the best-fit points of a former study of mSUGRA that has been performed by SFitter [26] and that used the same measurements as described in chapter 3. In order to embed these points into the NMSSM, we will apply also the additional mSUGRA specific constraints to the semi constrained NMSSM. For the actual transition to mSUGRA we decouple the singlet by setting the coupling λ to a value close to zero, which should finally result in the same predictions of the mass spectrum as mSUGRA. As we expect to find the same results as for mSUGRA, this allows us in addition to test the implementation of the software and to compare the underlying algorithms of the two programs SuSpect and NMSSMTools.

5.1 The NMSSM in the MSSM Limit

We shortly review the results of the mSUGRA study that has been performed by SFitter [26]. For the results that we will refer to, the sign of μ has been fixed to $+1$. The fit has been done for $m_0 < 5\,\text{TeV}$, $m_{1/2} < 5\,\text{TeV}$, $\tan\beta < 60$ and $-4\,\text{TeV} < A_0 < 4\,\text{TeV}$. In addition the top mass is free to vary within the error of its measurement. The result of the fit is displayed in Fig. 5.1 that shows the profile likelihood projections on the m_0-$m_{1/2}$-plane and the $m_{1/2}$-$\tan\beta$-plane. The z-axis parametrizes the likelihood.

	m_0	$m_{1/2}$	$\tan\beta$	A_0	m_t	μ
h-funnel	4232	135	26.6	-2925	174.2	484.4
A-funnel	1500	1700	46.5	2231	173.9	1560
τ-co-ann	442	999	24.6	-1347	174.0	1400

Table 5.1: Input parameters of mSUGRA best-fit points and result for μ

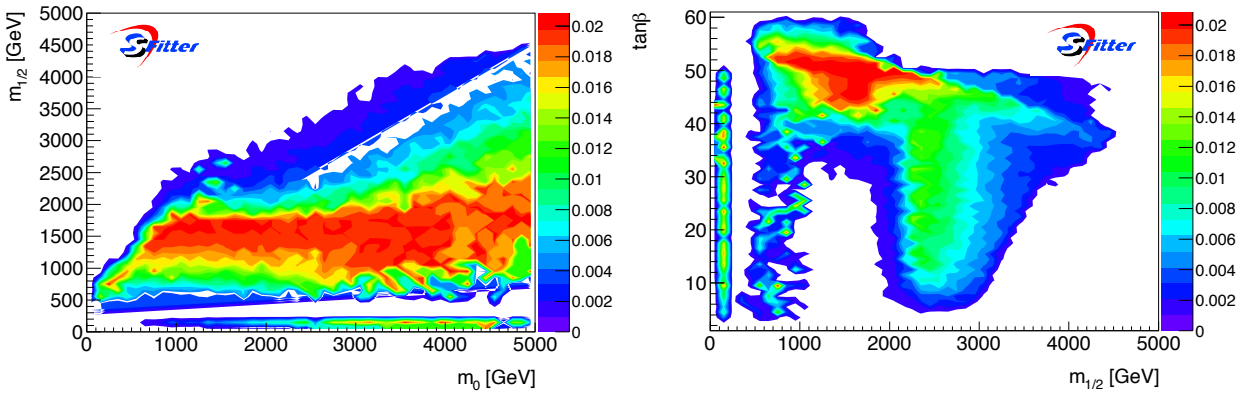

(a) (b)

Figure 5.1: Profile likelihood projections for mSUGRA fit on m_0-$m_{1/2}$-plane (a) and $m_{1/2}$-tan β-plane (b) from the SFitter paper [26].

One can identify three regions as described in section 2.4: The h funnel region with $m_{1/2} \approx 130\,\text{GeV}$, the A-funnel region with $m_{1/2} \approx 1.7\,\text{TeV}, 42 < \tan\beta < 55$ and the $\tilde{\tau}$-co-annihilation region with $m_{1/2} < 1\,\text{TeV}, m_0 < 1\,\text{TeV}$. Their best-fit points are listed in table 5.1. We start by emedding the best-fit points of the h and A-funnel region in the CNMSSM to test the stability of the underlying algorithms in the mSUGRA limit.

Now how do we come from the NMSSM to the mSUGRA limit?

So far we have introduced the semi constrained NMSSM. Compared to mSUGRA we have the additional parameters $\lambda, \kappa, A_\lambda, A_\kappa$ and $|\mu_{eff}|$ while m_0, $m_{1/2}$, $\tan\beta$, A_0, m_t and the sign of μ_{eff} are given by the best-fit point. In contrast to mSUGRA the semi constrained NMSSM does not assume the unification of $m^2_{H_u}$ and $m^2_{H_d}$ at the GUT scale. Assuming their unification to m_0 gives two additional conditions that reduce the number of free parameters by κ and $|\mu_{eff}|$.

Furthermore we have not assumed the unification of A_λ, A_κ. As they are free parameters, we have the freedom to be consistent and unify them by setting $A_\lambda = A_\kappa = A_0$ in the input. The only free parameter left is λ, the coupling between the singlet and the Higgs doublets.

In order to go to the limit of mSUGRA we have to decouple the singlet from the supersymmetric sector and hence from the Higgs doublets. This is done by setting λ to a very small value, 10^{-16}.

Applying all constraints eliminates all degrees of freedom and should reproduce the mSUGRA points. The results for the h-funnel point are listed in the third column in table 5.2.

Most of the sparticle masses have similar values as in the mSUGRA case. This is what we expect as the masses strongly depend on the input parameters m_0 for scalars and $m_{1/2}$ for the neutralinos and charginos. Nevertheless we find deviations

	mSUGRA	CNMSSM	
λ		10^{-16}	10^{-16}
m_t	174.2	174.2	175.4
κ		$1.408 \cdot 10^{-15}$	$5.775 \cdot 10^{-16}$
μ_{eff}	484.4	259.4	482.5
Ωh^2	0.1105	0.0209	0.0804
m_{h1}	123.84	121.9	122.2
m_{h2}	3626	3613	3633
m_{h3}		6534	4787
m_A	3626	3613	3633
m_{H^+}	3627	3614	3634
$m_{\chi_1^0}$	59.48	57.86	59.68
$m_{\chi_2^0}$	119	111	120
$m_{\chi_3^0}$	-504	-278	-502
$m_{\tilde{t}_1}$	2376	2429	2406
$m_{\tilde{g}}$	477	477	477

Table 5.2: Reproducing the best-fit h-funnel point with the constrained NMSSM

on the 10% level for the second neutralino and a factor of 2 difference between the two values for μ_{eff} and the mass of the third neutralino that is in a first approximation determined by μ_{eff}. With a value of 0.02 instead of 0.11 we observe the biggest deviation for the relic density. This is caused by the mass difference of the Higgs and the lightest neutralino as the h-funnel region is very sensitive to small deviations of the Higgs and the LSP mass.

The question remains why we observe this deviation. μ_{eff} is determined at the SUSY breaking scale in terms of the soft SUSY breaking parameters $m^2_{H_u}$ and $m^2_{H_d}$ that are only fixed at the GUT scale. The value of $m^2_{H_u}$ at the SUSY breaking scale is very sensitive to the top Yukawa coupling h_t as it is multiplied with the heavy stop mass. The codes of SuSpect and NMSSMTools differ in their algorithms that calculate the running of h_t that is closely connected to the mass of the top quark. Adjusting this mass can therefore bring μ_{eff} to the expected value as displayed in the third column. We observe that all other masses come closer to the values that have been computed by SuSpect. The mass differences are now all smaller than 2%. The mass of the third Higgs that appears in addition to mSUGRA decreases and makes it more accessible for BSM searches. Another effect is that the relic density has now a reasonable order of magnitude (0.08) which makes this point a good starting point for further studies.

A similar study has been performed for the A-funnel region. Table 5.3 displays the results. The first column for the CNMSSM shows the reproduced point with the same top mass for the CNMSSM. Again we observe deviations of more than 10%

Model	mSUGRA	CNMSSM	
λ		10^{-16}	10^{-16}
m_t	173.9	173.9	174.8
κ		$-8.4 \cdot 10^{-17}$	$-8.608 \cdot 10^{-17}$
μ_{eff}	1560	1603	1560
Ωh^2	0.1127	2.939	0.116
m_{h1}	123.03	120.17	120.8
m_{h2}	1498	1320	1498
m_{h3}		2066	2054
m_{A1}	1498	1319.6	1498
m_{H^+}	1500	1322	1500
$m_{\chi_1^0}$	744.6	740.9	740.9
$m_{\chi_2^0}$	1379	1380	1378
$m_{\chi_3^0}$	-1589	-1633	-1591
$m_{\tilde{t}_1}$	2771	2980	2958
$m_{\tilde{g}}$	3596	3607	3606

Table 5.3: Reproducing the best-fit A-funnel point with the constrained NMSSM

in the Higgs sector. The deviation on the mass $m_{A_1^0}$ leads to strong deviations in the relic density. It is increased by a factor of 30, as the annihilation through the A-funnel is not accessible.

The attempt to adjust the mass of the top quark does not lead to the desired corrections. Instead we fix the value for μ_{eff} to the one predicted by the mSUGRA point. Then we perform a two parameter fit for κ and the mass of the top quark, requiring $m_{A_1^0}$ to be around 1500. The result is displayed in the last column. Again we find an enhanced mass of the top quark with respect to the mSUGRA result from SuSpect due to the underlying algorithms. All values agree with the mSUGRA result within 5%. The price we have to pay for this is to loosen the constraint on the running Higgs masses. Instead of the unified value $m_0 = 1.5 \times 10^3$ we have now deviations of 6% for m_{H_u} and 17.0% for m_{H_d}.

5.2 Extending the h-funnel point

Starting from the point we found in section 5.1 we will now analyse the influence of the additional singlet in the h-funnel region. Therefore we loosen the applied constraints and go back from the constrained NMSSM to the semi constrained NMSSM. m_{H_u} and m_{H_d} no longer have to be unified. Instead we set μ_{eff} to the value of the best-fit point in table 5.1 and κ will be a fit parameter as λ. In addition A_λ and A_κ won't be unified but become free fit parameters. $m_0, m_{1/2}, A_0, \tan\beta$ are also set to the values of the best-fit point in table 5.1 and the mass of the top quark is adjusted to 175.4 GeV as found in section 5.1.

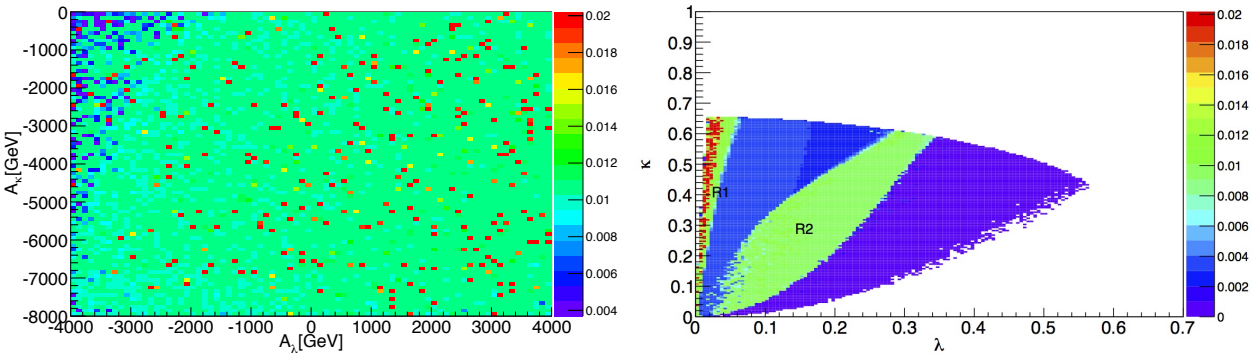

(a) (b)

Figure 5.2: Profile likelihood projections for semi constrained NMSSM fit on A_λ-A_κ-plane (a) and λ-κ-plane (b).

The range is set to $0 < \lambda, \kappa < 1, -4\,\text{TeV} < A_\lambda < 4\,\text{TeV}$ and $-8\,\text{TeV} < A_\kappa < 0\,\text{TeV}$. The results of the fit in terms of frequentist projections are displayed in Fig. 5.2. The projection on the A_λ-A_κ-plane shows a basically homogeneous distribution. Aside from a smaller region around $A_\lambda \approx -3\,\text{TeV}$ and $A_\kappa > -1\,\text{TeV}$ that has on average a smaller likelihood, we can not distinguish any substructures.

Fig. 5.2 (b) shows the projection on the λ-κ plane. In contrast to the A_λ-A_κ plane we find clear structures. First of all there is a wide area, coloured white, where SFitter finds only non valid results. This is caused by different problems depending on the area of the parameter space. For $\lambda < 0.02$ the stop mass squared becomes negative and for $\kappa < 0.4$ the quadratic Higgs mass becomes smaller than 0. These are unphysical results and are therefore not displayed. For the white region with $\kappa > 0.5$ the model has a Landau pole below the GUT scale which causes integration problems in the RGEs. Looking at the RGEs we have seen that λ and κ are strongly correlated:

$$16\pi^2 \frac{d\lambda^2}{d\ln Q^2} = 4\lambda^4 + 2\lambda^2\kappa^2 + \ldots \tag{5.1}$$

$$16\pi^2 \frac{d\kappa^2}{d\ln Q^2} = 6\kappa^4 + 6\kappa^2\lambda^2 + \ldots \tag{5.2}$$

On the one hand both couplings grow with Q^2. On the other hand they have to remain smaller than 1 up to the GUT scale where new physics has to enter. Otherwise the theory is no longer perturbative. Therefore we find maximum values for λ and κ. Moreover we observe a correlation between λ and κ for the maximal value. This is caused by the second term in the RGE where the couplings enter quadratically. One can state: the bigger κ the faster grows λ and vice versa. Therefore at

Observable	value	CNMSSM			
		R1	$\Delta\chi^2$	R2	$\Delta\chi^2$
m_h	126.0	125.25	0.00	120.18	24.83
Ωh^2	0.1187	0.1217	0.00	0.10768	0.00
a_μ	$2.87 \cdot 10^{-9}$	$6.3 \cdot 10^{-11}$	10.67	$4.6 \cdot 10^{-11}$	10.81
$BR(B \to X_s\gamma)$	$3.55 \cdot 10^{-4}$	$2.73 \cdot 10^{-4}$	10.15	$3.12 \cdot 10^{-4}$	2.87
$BR(B_s^0 \to \mu^+\mu^-)$	$3.2 \cdot 10^{-9}$	$3.8 \cdot 10^{-9}$	0.07	$3.8 \cdot 10^{-9}$	0.07
$BR(B^+ \to \tau^+\nu)$	$1.41 \cdot 10^{-4}$	$1.32 \cdot 10^{-4}$	0.05	$1.32 \cdot 10^{-4}$	0.05
Δm_{B^0}	0.51	0.63	0.00	0.62	0.00
$\Delta m_{B_s^0}$	17.69	21.94	0.00	21.33	0.00
$\Gamma_{Z\to Inv}$	-1.9	0.00	1.36	0.00	1.36
$\Gamma_{Z\to Higgs}$	6.5	0.00	5.72	0.00	5.72
m_t	173.5	175.4	3.61	175.4	3.61
χ^2			44.912		68.33

Table 5.4: Best-fit points for R1 and R2.

the limit we observe smaller values of κ for bigger values of λ.

Next we consider the actually accessible parameter space. Here we can identify two regions that do not overlap. The first narrow region (R1) is characterized by a constant ratio of κ/λ.

It is limited by $10 \lesssim \kappa/\lambda \lesssim 40$ with the most likely configuration of $17 \lesssim \kappa/\lambda \lesssim 30$. For small values of λ R1 limits at the same time the fully accessible region in the λ-κ-parameter space. The second region (R2) has a lower limit of $0.015 < \kappa$ which distinguishes it from R1 that is not limited from below. Besides R2 is not limited by linear correlation but evolves with deviations around $\kappa/\lambda \approx 2.0$.

Comparing best-fit points from different runs in the blue area reveals, that the high χ^2 is caused by deviations from the relic density. As we are in the h-funnel region the relic density is highly sensitive to the masses of the lightest Higgs h_1 and the LSP χ_1^0. Fixing κ to 0.5 and fitting A_λ and A_κ for $\lambda = 0.05$ (R1), 0.15 (blue) and 0.2 (R2) shows that the difference comes from small differences in the Higgs mass, that varies by 0.4 GeV while the mass of the LSP only varies by less than 0.1 GeV. From $\kappa = 0.05$ to 0.15 the Higgs mass increases by 0.2 GeV while the LSP mass decreases by 0.06 GeV which brings them closer to the on-shell condition. Therefore the annihilation cross section increases and the relic density becomes too small. For $\kappa = 0.2$ the Higgs mass decreases again by 0.4 GeV to a smaller value than for $\kappa = 0.05$ resulting again in the correct relic density.

As the observed structures depend on the LSP and the Higgs mass, we can explain them by looking at the calculation of their masses. As mentioned in section 2.2.2 the LSP mass is basically set by $m_{1/2}$ and depends only indirectly on κ and

λ. The tree level Higgs mass matrix on the other hand clearly depends on the ratio κ/λ at the tree level. Here one expects a stronger dependence on the NMSSM parameters which is also in agreement with the observation. We can therefore state that the measurements of the relic density and the Higgs mass still select narrow regions of the parameter space even though we have added four additional parameters.

To analyse the likelihood of the two regions we consider the uncorrelated contributions to χ^2 that is related to the likelihood by $\chi^2 = -2 \log L$. The best-fit points in table 5.4 show how the observables aside from the Higgs couplings contribute to the total χ^2 of 44.9 for R1 and 68.3 for R2. For both regions Ωh^2 is the measurement that has the highest influence on the likelihood map. Deviations from the funnel region and the resulting deviations of the relic density can lead to χ^2 contributions several orders of magnitude higher than the best fit result. Therefore the best-fit points are in agreement with the experimental outcome. The predictions are also in agreement with $\Delta m_{B_s^0}$ and Δm_{B^0} due to the large theoretical uncertainty of the SUSY calculations. For $\Gamma_{Z \to Inv}$ and $\Gamma_{Z \to Higgs}$ we do not observe any contributions from the NMSSM due to the LSP and Higgs masses that are too high for decay products of the Z boson. The contribution from the top mass is of course also the same for both points.

For the other observables the deviations from the experiments differ between the two regions. For the first region the Higgs mass lies in the allowed range and therefore the contribution from this measurement is zero. The main contributions to χ^2 come from a_μ and $BR(B \to X_s\gamma)$ where the NMSSM contributions that are supposed to enhance the SM values are systematically too small. The χ^2 contributions from the Higgs channels are not listed. All contributions to χ^2 are of order one or less and therefore compatible. For the second region the main contributions come from the Higgs mass, that is too small, and again from the anomalous magnetic moment. The diagonal entries of the CP even Higgs mass matrix show a positive dependence on κ/λ that might cause the smaller Higgs mass for the smaller ratio of κ/λ in this region. The deviation from the observed Higgs mass also results in higher deviations for the couplings which again result in a bigger total χ^2. So we find that the second region is more favourable for the B-Physics observables but the deviations from the measured Higgs mass make it overall less likely.

After analysing the χ^2 contribution of the best-fit points of the two regions we want to know which influence the singlet has on R1 and R2. Due to the singlet we have an additional neutralino, a CP even and a CP odd Higgs. As we are in the h-funnel region, we can observe the influence of the singlet via the CP even Higgs sector. We set an additional constraint on the Higgs mixing matrix H_{MIX}. First we require the heaviest Higgs to be mainly singlet by setting $H_{MIX,33} > 0.99$. The fit result is displayed in figure 5.3(a). For another fit we do the same for the second Higgs, setting $H_{MIX,23} > 0.99$ (Fig. 5.3 (b)). Finally we require a minimal contribution to the lightest Higgs $H_{MIX,13} > 0.02$ (Fig. 5.4).

We observe that the first constraint reproduces most of R1 while R2 remains

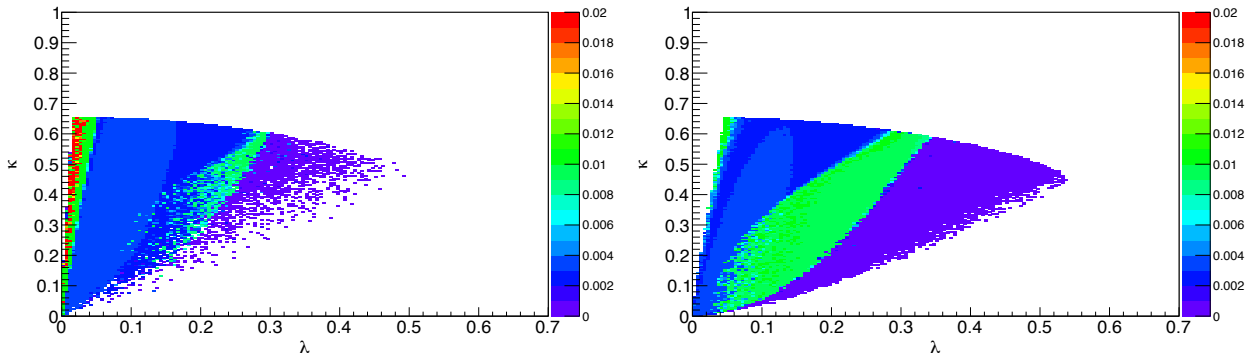

(a) (b)

Figure 5.3: Profile likelihood projections on λ, κ plane for semi constrained NMSSM fit with additional constraints on the Higgs mixing matrix: singlet like h_3 (a) and singlet like h_2 (b)

accessible but only with poor results. So we isolate the region that contains the reproduced mSUGRA point. This is in agreement with the expectation that the constraint enforces a decoupled singlet and as soon as the singlet-like Higgs has no impact on the SUSY sector we observe a mSUGRA like phenomenology.

When applying the first constraint, that decouples the singlet R1 is not fully recovered but only up to $\kappa/\lambda > 13$. The second constraint gives back R2 and the missing part of R1 a small band with $10 < \kappa/\lambda < 13$, that is the limit of the accessible parameter space. Thus a combination of both fits would recover the whole region of R1.

Applying the third constraint, that requires a singlet contribution to the lightest Higgs, leads to a strongly reduced parameter space. R1 is not included anymore and R2 is reduced to $\lambda < 0.3$

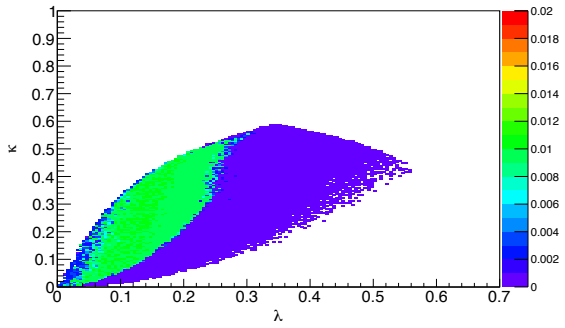

Figure 5.4: Profile likelihood projection on λ, κ plane for semi constrained NMSSM fit with singlet contribution to the lightest Higgs by requiring $H_{MIX,13} > 0.02$

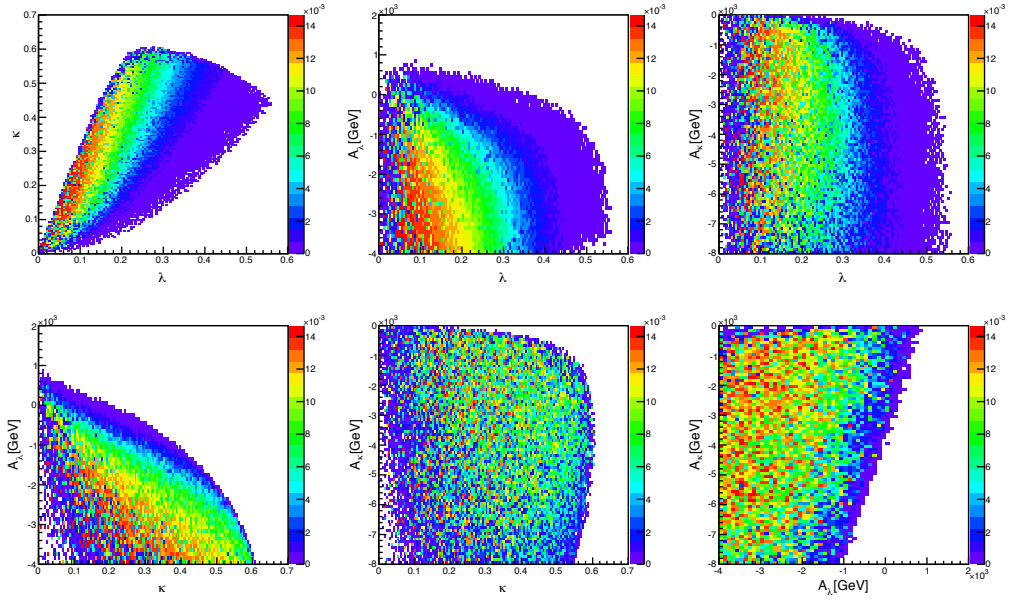

Figure 5.5: Profile likelihood fit for the best-fit point of the mSUGRA A-funnel region. $0 < \lambda, \kappa < 1$, $-4\,\text{TeV} < A_\lambda < 2\,\text{TeV}$ and $-8\,\text{TeV} < A_\kappa < 0\,\text{TeV}$.

Summing up we found two regions in the λ-κ-plane (see Fig. 5.2(b)). One includes the reproduced mSUGRA point and reproduces its properties. The second has a singlet like second Higgs, which hints at additional solutions due to the NMSSM, but does not describe data as well as the first one.

5.3 Extending the A-funnel Point

After investigating the h-funnel region, the question arises whether the A-funnel region behaves the same way, providing a second region due to a singlet like A_2^0. As for the h-funnel point we set $m_0, m_{1/2}, A_0, \tan\beta, \mu_{eff}$ and m_t to the best-fit point parameters and the input parameters found to reproduce this point. Then we perform a fit over the singlet related parameters setting $0 < \lambda, \kappa < 1$, $-4\,\text{TeV} < A_\lambda < 2\,\text{TeV}$ and $-8\,\text{TeV} < A_\kappa < 0\,\text{TeV}$.

Figure 5.5 shows again a linear correlation between λ and κ. In addition A_λ is correlated to both couplings. The linear correlation of λ and κ can again be explained by looking at the A mass matrix. As for the H mass matrix κ only appears in the ratio κ/λ, even though we also observe λ as a global factor in the off diagonal and the second diagonal entry. This explains again the linear correlation between the two parameters. For A_λ the correlation can not be determined from first principles. It appears on tree level only in sums with $\mu_{eff}\kappa/\lambda$ and different prefactors. In addition the input parameter for A_λ, that is displayed in the fit, is given at the

Observable	Measurement	NMSSM prediction	$\Delta\chi^2$
m_h	126.0	120.80	15.17
Ωh^2	0.1187	0.1285	0.00
m_{A_0}		1505	
$m_{\chi_1^0}$		740.9	
a_μ	$2.87 \cdot 10^{-9}$	$2.13 \cdot 10^{-10}$	9.48
$BR(B \to X_s\gamma)$	$3.55 \cdot 10^{-4}$	$3.23 \cdot 10^{-4}$	1.56
$BR(B_s^0 \to \mu^+\mu^-)$	$3.2 \cdot 10^{-9}$	$2.3 \cdot 10^{-9}$	0.21
$BR(B^+ \to \tau^+\nu)$	$1.41 \cdot 10^{-4}$	$1.26 \cdot 10^{-4}$	0.11
Δm_{B^0}	0.51	0.61	0.00
$\Delta m_{B_s^0}$	17.69	21.13	0.00
$\Gamma_{Z\to Inv}$	-1.9	0	1.36
$\Gamma_{Z\to Higgs}$	6.5	0	5.72
m_t	173.5	174.8	1.69
χ^2			54.19

Table 5.5: Best-fit point for the A-funnel region.

GUT scale, while the mass matrix is calculated at the electroweak scale. Figure 5.5 therefore shows a correlation that is in principle expected but not predictable in details. Concerning A_κ we observe no correlation in the region with enhanced likelihood.

The χ^2 contributions of the best-fit point in table 5.5 indicate strengths and weaknesses of this region compared to the h-funnel region.

As for the h-funnel the relic density is the constraining parameter, that reduces the acceptable region to the parameter space that reproduces the correct relic density. There Ωh^2 is in agreement with the measurement. For the anomalous magnetic moment we find the same difficulties in producing sufficient contributions to loop corrections, but we can at least detect sizeable contributions of 7% of the measured value. The branching ratio $BR(B \to X_s\gamma)$, that was one of the main contributions in the h-funnel point, has acquired sufficient contributions to reduce the χ^2 to 1.6. The discussed variable all provide the same or a better agreement with measurements and the additional contributions due to B-physics, the top quark mass and electroweak precision data are also comparable.

The only problematic parameter is the mass of the lightest Higgs, that is too light. This leads not only too a strong deviation from the observed Higgs mass but also to further deviations due to the couplings. Including these discrepancies we find a total χ^2 of 54.19 that is higher then the value found for the mSUGRA like h-funnel region but smaller than the χ^2 found for R2.

A second fit that allows for negative couplings by setting $-1 < \lambda, \kappa < 1$ and $-3\,\text{TeV} < A_\lambda, A_\kappa < 3\,\text{TeV}$ leads to the results displayed in Fig. 5.6. We see the

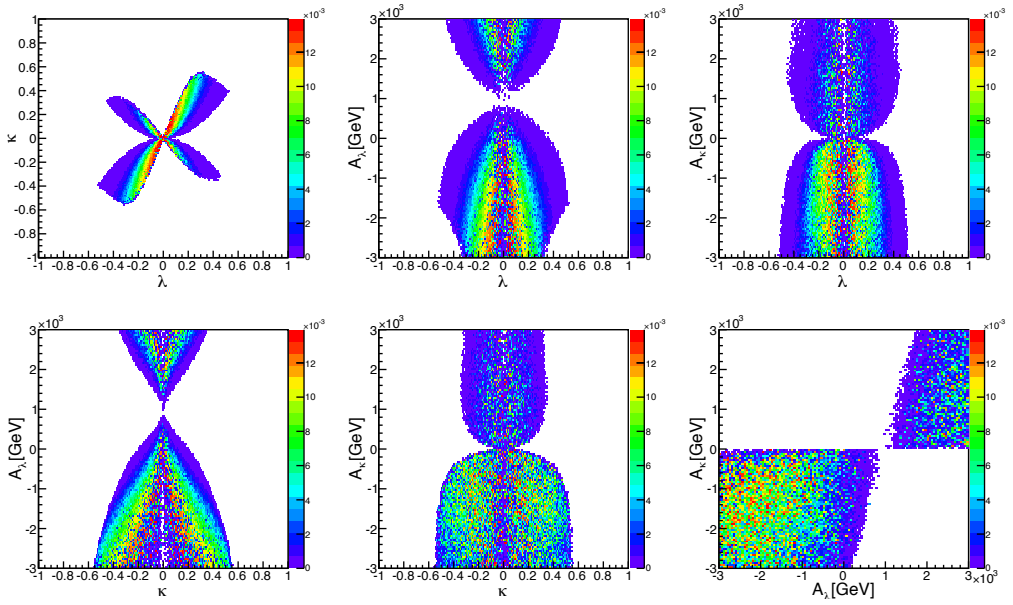

Figure 5.6: Profile likelihood fit for the best-fit point of the mSUGRA A-funnel region. $-3\,\text{TeV} < A_\lambda, A_\kappa < 3\,\text{TeV}$ and $-1 < \lambda, \kappa < 1$.

symmetric form that is determined by the signs of the couplings and the corresponding SUSY breaking trilinear couplings. We find the following correlation: if λ and κ have the same sign, A_κ is negative and A_λ is smaller than 1 TeV. Otherwise A_κ is positive and A_λ is larger than 1 TeV.

Summarizing we can state that also in the extension of the A-funnel best-fit point the measurements only allow for narrow regions in the λ-κ-plane and imply a strong correlation between A_λ and the couplings.

6 Conclusion and Outlook

For the study of the NMSSM by SFitter we have implemented NMSSMTools for SFitter.

The software has been tested in the MSSM limit of a decoupled singlet. We used two different ways to embed the best fit points of the h- and A-funnel region of mSUGRA into a constrained version of the NMSSM. For the h-funnel we were able to apply the full constraints from mSUGRA plus the additional unification of A_λ and A_κ. Differences in algorithms between SuSpect and NMSSMTools required an adjustment of the top quark mass due to its impact on the μ parameter. This way we were able to embed the point into the CNMSSM and find a mass spectrum that is compatible with the mSUGRA point within 5%.

For the A-funnel we had to release the unification of the soft Higgs masses and do a fit over the top quark mass and the self-coupling κ to find a point with the correct mass spectrum. Comparing both methods the first one appears as the more natural choice to embed mSUGRA into the semi-constrained NMSSM, but its success clearly depends on the region in parameter space.

Starting from the embedded points we have studied the impact of the additional parameter space with respect to the MSSM that opens due to the singlet.

In the λ-κ-plane of the h-funnel's best fitting point we found two regions. One is the continuation of the mSUGRA h-funnel point, that is characterized by a decoupled singlet that leads to a heavy singlet-like third Higgs boson. Moreover we found a second region with smaller ratio of κ/λ, that provides the right ratio of neutralino and Higgs mass to obtain a relic density within the allowed limits. This solution arises when the singlet contributes to the Higgs sector and is characterised by a singlet like second Higgs boson. The region has a smaller mass of the lightest Higgs boson which decreases its likelihood. A possible reason is the influence of a smaller ratio of κ/λ on the tree level mass.

For the A-funnel the best fitting point also opens into a region in the λ-κ-plane. The parameter space corresponds again to a special ratio of κ over λ. The best-fit point has a smaller likelihood than the best fit point in the h-funnel region due to the smaller Higgs mass. In addition we found a sizeable region with mixed signs of the coupling constants. The regions are symmetric for simultaneous sign exchange in λ and κ and around the A_λ-value of 1 TeV.

The analysis of the h-funnel region gave hints at additional parameter configurations that provide the correct the relic density. At the same time we found, that the measurements of the Higgs mass and the relic density select only narrow re-

gions of the parameter space instead of leaving the whole parameter space available due to the additional parameters. A first step into further analysis is the study of the remaining $\bar{\tau}$-co-annihilation region that has been found by the mSUGRA study. In a next step one would release the parameters of the constrained and the semi-constrained NMSSM for a full scan. The present study revealed strong correlations e.g. between λ and κ and gave us a principle idea of their behaviour. So for a global fit including all parameters we would expect that again not all of the parameter space remains accessible but that we find structures and correlations between input parameters like λ and κ.

Das machen wir…

Another possibility is the implementation of a new model, a low scale NMSSM with an larger parameter space. It will be interesting to see whether the measurements are even here able to select certain regions or whether it finally becomes impossible to find substructures due to the high number of parameters.

…und das machen wir nicht.

Acknowledgement

This master thesis is the result of a one year work at University Paris Sud and it would not have been realized without the support of many people I would like to thank.

First of all I would like to thank my supervisors, Dr. Dirk Zerwas and Prof. Dr. Tilman Plehn for their support. Tilman, thank you very much for motivating me to go abroad and making this whole project possible. Dirk, it was a pleasure to work and discuss with you and I would like to thank you for always being available and still giving me enough freedom to develop my own ideas.

I would like to thank Michael Rauch and Rémi Lafaye for their technical support about SFitter and Cyril Hugonie and Ulrich Ellwanger for answering all my questions about NMSSMTools and the NMSSM in general.

I would like to thank the laboratory, its administration and Geneviève. I would especially like to thank the ATLAS group for the hospitality, the warm welcome and the technical support they provided me.

A special thanks goes to Estelle, my most favourite office mate for the company, the encouraging support and the coffee breaks that never needed coffee. In addition I would like to thank Laurent Duflot, Sophie Henrot-Versille, Marija Marjanovic and Nikola Makovec for the numerous discussions about SUSY and technical problems, the endless attempts to finally read the primer and great support in various aspects of life - the heater saved my life!

Furthermore, I would like to thank in chronological order Simon, Jessi, Violeta, Reimar, Milla and Vincent who made me enjoy this year in so many ways.

Guillaume, I would like to thank you for making me enjoy great times and for making me laugh even during the worst ones. You made me feel at home in your country and I hope I will manage to do the same for you.

Last but not least, I would like to thank my parents who have supported me at all stages of my life. I could not wish for more.

I would like to dedicate this thesis to my grandma, who had to leave this world while I was writing the last lines of this thesis. I will always miss you.

Part I

Appendix

A Lists

A.1 List of Figures

A.2 List of Tables

B Bibliography

[1] S. Weinberg, Phys. Rev. Lett. **19** (1967) 1264. S. L. Glashow, Nucl. Phys. **22** (1961) 579.

[2] P. A. R. Ade *et al.* [Planck Collaboration], arXiv:1303.5076 [astro-ph.CO].

[3] Particle Data Group http://pdg.lbl.gov/2012/reviews/rpp2012-rev-g-2-muon-anom-mag-moment.pdf

[4] P. W. Higgs, Phys. Lett. **12**, 132 (1964); P. W. Higgs, Phys. Rev. Lett. **13**, 508 (1964); F. Englert and R. Brout, Phys. Rev. Lett. **13**, 321 (1964); ATLAS Collaboration, Phys. Lett. B **716**, 1 (2012); CMS Collaboration, Phys. Lett. B **716**, 30 (2012).

[5] for reviews of the MSSM see *e.g.* S. P. Martin, In *Kane, G.L. (ed.): Perspectives on supersymmetry II* 1-153 [hep-ph/9709356]. I. J. R. Aitchison, arXiv:hep-ph/0505105.

[6] P. Fayet and S. Ferrara, Phys. Rept. **32** (1977) 249. P. Fayet, Phys. Lett. B **69** (1977) 489.

[7] S. Dimopoulos and H. Georgi, Nucl. Phys. B **193** (1981) 150.

[8] J. R. Ellis, J. F. Gunion, H. E. Haber, L. Roszkowski and F. Zwirner, Phys. Rev. D **39** (1989) 844.

[9] R. Lafaye, T. Plehn and D. Zerwas, arXiv:hep-ph/0404282; R. Lafaye, T. Plehn, M. Rauch and D. Zerwas, Eur. Phys. J. C **54**, 617 (2008).

[10] T. Plehn, Lect. Notes Phys. **886** (2015).

[11] G. Altarelli and F. Feruglio, Springer Tracts Mod. Phys. **190** (2003) 169 [hep-ph/0206077].

[12] L. E. Ibañez, Phys. Lett. B **118**, 73 (1982); J. R. Ellis, D. V. Nanopoulos and K. Tamvakis, Phys. Lett. B **121**, 123 (1983); L. Alvarez-Gaumé, J. Polchinski and M. B. Wise, Nucl. Phys. B **221**, 495 (1983); K. Inoue, A. Kakuto, H. Komatsu and S. Takeshita, Prog. Theor. Phys. **68**, 927 (1982) [Erratum-ibid. **70**, 330 (1983)]; A. H. Chamseddine, R. Arnowitt and P. Nath, Phys. Rev. Lett. **49**, 970 (1982).

[13] for early studies see *e.g.* M. S. Carena, J. R. Espinosa, M. Quiros and C. E. M. Wagner, Phys. Lett. B **355**, 209 (1995); H. E. Haber, R. Hempfling and A. H. Hoang, Z. Phys. C **75**, 539 (1997); S. Heinemeyer, W. Hollik and G. Weiglein, Eur. Phys. J. C **9**, 343 (1999); G. Degrassi, S. Heinemeyer, W. Hollik, P. Slavich and G. Weiglein, Eur. Phys. J. C **28**, 133 (2003).

[14] M. L. Brooks *et al.* [MEGA Collaboration], Phys. Rev. Lett. **83** (1999) 1521 [hep-ex/9905013].

[15] H. Goldberg, Phys. Rev. Lett. **50**, 1419 (1983); M. Drees and M. M. Nojiri, Phys. Rev. D **47**, 376 (1993); J. R. Ellis, J. S. Hagelin, D. V. Nanopoulos, K. A. Olive and M. Srednicki, Nucl. Phys. B **238**, 453 (1984); G. Jungman, M. Kamionkowski and K. Griest, Phys. Rept. **267**, 195 (1996); G. Bertone, D. Hooper and J. Silk, Phys. Rept. **405**, 279 (2005).

[16] S. Dawson and H. Georgi, Phys. Rev. Lett. **43**, 821 (1979); M. B. Einhorn and D. R. T. Jones, Nucl. Phys. B **196**, 475 (1982); U. Amaldi, W. de Boer and H. Furstenau, Phys. Lett. B **260**, 447 (1991). J. R. Ellis, S. Kelley and D. V. Nanopoulos, Phys. Lett. B **260** (1991) 131. P. Langacker and M. x. Luo, Phys. Rev. D **44** (1991) 817.

[17] B. A. Dobrescu, K. Kong and R. Mahbubani, Phys. Lett. B **670**, 119 (2008); M. Gerbush, T. J. Khoo, D. J. Phalen, A. Pierce and D. Tucker-Smith, Phys. Rev. D **77**, 095003 (2008); T. Plehn and T. M. P. Tait, J. Phys. G **36**, 075001 (2009); S. Y. Choi, M. Drees, J. Kalinowski, J. M. Kim, E. Popenda and P. M. Zerwas, Phys. Lett. B **672**, 246 (2009); ATLAS Collaboration, Eur. Phys. J. C **73**, 2263 (2013). [arXiv:1210.4826 [hep-ex]].

[18] G. F. Giudice and A. Masiero, Phys. Lett. B **206** (1988) 480.

[19] U. Ellwanger, C. Hugonie and A. M. Teixeira, Phys. Rept. **496** (2010) 1 [arXiv:0910.1785 [hep-ph]].

[20] J. A. Aguilar-Saavedra, A. Ali, B. C. Allanach, R. L. Arnowitt, H. A. Baer, J. A. Bagger, C. Balazs and V. D. Barger *et al.*, Eur. Phys. J. C **46**, 43 (2006). [hep-ph/0511344].

[21] K. Griest and D. Seckel, Phys. Rev. D **43**, 3191 (1991); S. Mizuta and M. Yamaguchi, Phys. Lett. B **298**, 120 (1993); J. R. Ellis, T. Falk and K. A. Olive, Phys. Lett. B **444**, 367 (1998); J. R. Ellis, T. Falk, K. A. Olive and M. Srednicki, Astropart. Phys. **13**, 181 (2000) [Erratum-ibid. **15**, 413 (2001)].

[22] J. R. Ellis, K. A. Olive and Y. Santoso, Astropart. Phys. **18**, 395 (2003).

[23] P. Binetruy, G. Girardi and P. Salati, Nucl. Phys. B **237**, 285 (1984); S. Mizuta and M. Yamaguchi, Phys. Lett. B **298**, 120 (1993); J. Edsjo and P. Gondolo, Phys. Rev. D **56**, 1879 (1997).

[24] T. Cohen and J. G. Wacker, JHEP **1309** (2013) 061 [arXiv:1305.2914 [hep-ph]].

[25] J. L. Feng, K. T. Matchev and F. Wilczek, Phys. Lett. B **482**, 388 (2000). J. L. Feng and F. Wilczek, Phys. Lett. B **631** (2005) 170 [hep-ph/0507032].

[26] S. Henrot-Versillé, R. Lafaye, T. Plehn, M. Rauch, D. Zerwas, S. Plaszczynski, B. Rouillé d'Orfeuil and M. Spinelli, Phys. Rev. D **89** (2014) 055017 [arXiv:1309.6958 [hep-ph]].

[27] J. M. Butterworth, A. R. Davison, M. Rubin and G. P. Salam, Phys. Rev. Lett. **100** (2008) 242001 [arXiv:0802.2470 [hep-ph]].

[28] ATLAS Collaboration, Phys. Lett. B **710** 383 (2012); ATLAS Collaboration, Phys. Rev. Lett. **108** 111803 (2012); ATLAS Collaboration, Phys. Lett. B **716** 62 (2012); ATLAS Collaboration, JHEP **1209** 070 (2012) ; ATLAS Collaboration, Phys. Rev. D **86** 032003 (2012); ATLAS Collaboration, Phys. Lett. B **716** 1 (2012) ; CMS Collaboration, Phys. Lett. B **710** 91 (2012) ; CMS Collaboration, Phys. Rev. Lett. **108** 111804 (2012); CMS Collaboration, Phys. Lett. B **710** 284 (2012); CMS Collaboration, Phys. Lett. B **713** 68 (2012).

[29] D. J. Fixsen, Astrophys. J. **707** (2009) 916 [arXiv:0911.1955 [astro-ph.CO]].

[30] G. Hinshaw *et al.* [WMAP Collaboration], arXiv:1212.5226 [astro-ph.CO].

[31] C. l. Kuo *et al.* [ACBAR Collaboration], Astrophys. J. **600** (2004) 32 [astro-ph/0212289].

[32] T. J. Pearson, B. S. Mason, A. C. S. Readhead, M. C. Shepherd, J. L. Sievers, P. S. Udomprasert, J. K. Cartwright and A. J. Farmer *et al.*, Astrophys. J. **591** (2003) 556 [astro-ph/0205388].

[33] D. N. Spergel *et al.* [WMAP Collaboration], Astrophys. J. Suppl. **148** (2003) 175 [astro-ph/0302209].

[34] C. L. Bennett *et al.* [WMAP Collaboration], arXiv:1212.5225 [astro-ph.CO].

[35] C. L. Reichardt, R. de Putter, O. Zahn and Z. Hou, Astrophys. J. **749**, L9 (2012); S. Das, T. Louis, M. R. Nolta, G. E. Addison, E. S. Battistelli, J R. Bond, E. Calabrese and D. C. M. J. Devlin *et al.*, arXiv:1301.1037 [astro-ph.CO].

[36] F. Beutler, C. Blake, M. Colless, D. H. Jones, L. Staveley-Smith, L. Campbell, Q. Parker and W. Saunders *et al.*, Mon. Not. Roy. Astron. Soc. **416**, 3017 (2011); N. Padmanabhan, X. Xu, D. J. Eisenstein, R. Scalzo, A. J. Cuesta, K. T. Mehta and E. Kazin, Mon. Not. Roy. Astron. Soc. **427**, no. 3, 2132 (2012); L. Anderson, E. Aubourg, S. Bailey, D. Bizyaev, M. Blanton, A. S. Bolton, J. Brinkmann and J. R. Brownstein *et al.*, Mon. Not. Roy. Astron. Soc. **427**, no. 4, 3435 (2013).

[37] G. W. Bennett *et al.* [Muon G-2 Collaboration], Phys. Rev. D **73** (2006) 072003 [hep-ex/0602035].

[38] for a review on new–physics effects see *e.g.* D. Stöckinger, J. Phys. G **34**, R45 (2007).

[39] Particle Data Group http://pdg.lbl.gov/2012/reviews/rpp2012-rev-b-meson-prod-decay.pdf

[40] M. Misiak, H. M. Asatrian, K. Bieri, M. Czakon, A. Czarnecki, T. Ewerth, A. Ferroglia and P. Gambino *et al.*, Phys. Rev. Lett. **98** (2007) 022002 [hep-ph/0609232].

[41] T. Becher and M. Neubert, Phys. Rev. Lett. **98** (2007) 022003 [hep-ph/0610067].

[42] R. Aaij *et al.* [LHCb Collaboration], Phys. Rev. Lett. **110**, 021801 (2013).

[43] D. Asner *et al.* [Heavy Flavor Averaging Group Collaboration], arXiv:1010.1589 [hep-ex].

[44] Particle Data Group: http://pdg.lbl.gov/2014/listings/rpp2014-list-z-boson.pdf

[45] Particle Data Group: http://pdg.lbl.gov/2012/reviews/rpp2012-rev-standard-model.pdf

[46] C. Adam, J. -L. Kneur, R. Lafaye, T. Plehn, M. Rauch and D. Zerwas, Eur. Phys. J. C **71**, 1520 (2011); E. Turlay, R. Lafaye, T. Plehn, M. Rauch and D. Zerwas, J. Phys. G **38**, 035003 (2011).

[47] R. Lafaye, T. Plehn, M. Rauch, D. Zerwas and M. Dührssen, JHEP **0908**, 009 (2009); M. Klute, R. Lafaye, T. Plehn, M. Rauch and D. Zerwas, Phys. Rev. Lett. **109**, 101801 (2012); D. Lopez-Val, T. Plehn and M. Rauch, arXiv:1308.1979 [hep-ph].

[48] A. Höcker, H. Lacker, S. Laplace and F. Le Diberder, Eur. Phys. J. C **21**, 225 (2001).

[49] A. Gelman and D. B. Rubin, Statist. Sci. **7** 457 (1992).

[50] B. C. Allanach and C. G. Lester, Phys. Rev. D **73** 015013 (2006).

[51] F. James and M. Roos, Comput. Phys. Commun. **10**, 343 (1975).

[52] A. Djouadi, J. -L. Kneur and G. Moultaka, Comput. Phys. Commun. **176**, 426 (2007).

[53] A. Djouadi, J. Kalinowski and M. Spira, Comput. Phys. Commun. **108**, 56 (1998); M. Mühlleitner, A. Djouadi and Y. Mambrini, arXiv:hep-ph/0311167; A. Djouadi, M. M. Mühlleitner and M. Spira, Acta Phys. Polon. B **38**, 635 (2007).

[54] S. Heinemeyer, W. Hollik, A. M. Weber and G. Weiglein, JHEP **0804**, 039 (2008). A. Weber, private communication.

[55] U. Ellwanger, J. F. Gunion and C. Hugonie, JHEP **0502** (2005) 066 [hep-ph/0406215]. U. Ellwanger and C. Hugonie, Comput. Phys. Commun. **175** (2006) 290 [hep-ph/0508022]. G. Belanger, F. Boudjema, C. Hugonie, A. Pukhov and A. Semenov, JCAP **0509** (2005) 001 [hep-ph/0505142].

[56] U. Ellwanger and C. Hugonie, Comput. Phys. Commun. **177** (2007) 399 [hep-ph/0612134].

[57] U. Ellwanger, C.-C. Jean-Louis and A. M. Teixeira, JHEP **0805** (2008) 044 [arXiv:0803.2962 [hep-ph]].

[58] D. Das, U. Ellwanger and A. M. Teixeira, Comput. Phys. Commun. **183** (2012) 774 [arXiv:1106.5633 [hep-ph]]. M. Muhlleitner, A. Djouadi and Y. Mambrini, Comput. Phys. Commun. **168** (2005) 46 [hep-ph/0311167].

[59] G. Belanger, F. Boudjema, P. Brun, A. Pukhov, S. Rosier-Lees, P. Salati and A. Semenov, Comput. Phys. Commun. **182**, 842 (2011).

Erklärung:

Ich versichere, dass ich diese Arbeit selbstständig verfasst habe und keine anderen als die angegebenen Quellen und Hilfsmittel benutzt habe.

Heidelberg, den (Datum) .....